Research Paper

GEOSPHERE

GEOSPHERE, v. 15, no. 2

https://doi.org/10.1130/GES01649.1

10 figures; 1 set of supplemental files

CORRESPONDENCE: li.lin8611@gmail.com

CITATION: Li, L., Garzione, C.N., Fan, M.J., Li, X.W., and Li, X.Z., 2019, Jurassic sedimentation in the south-central Qiangtang terrane reveals successive terrane collisions in central Tibet: Geosphere, v. 15, no. 2, p. 433–449, https://doi.org/10.1130/GES01649.1.

Science Editor: Shanaka de Silva
Associate Editor: Michael H. Taylor

Received 15 December 2017
Revision received 26 September 2018
Accepted 14 December 2018

Published online 29 January 2019

Jurassic sedimentation in the south-central Qiangtang terrane reveals successive terrane collisions in central Tibet

Lin Li[1,*], Carmala N. Garzione[2], Majie Fan[1], Xiaowei Li[3], and Xiangzhong Li[4]

[1]Department of Earth and Environmental Sciences, University of Texas at Arlington, Arlington, Texas 76019, USA
[2]Department of Earth and Environmental Sciences, University of Rochester, Rochester, New York 14627, USA
[3]State Key Laboratory of Geological Processes and Mineral Resources, School of Earth Sciences and Resources, China University of Geosciences, Beijing 100083, China
[4]Institute of Earth Environment, Chinese Academy of Sciences, Xi'an 710075, China

ABSTRACT

Our limited knowledge of Mesozoic tectonism in the Tibetan Plateau has hindered understanding of its geologic evolution. This study uses zircon U-Pb geochronology to refine regional chronostratigraphy and infer the Jurassic sedimentary-tectonic evolution of the Bangong suture and the south-central Qiangtang terrane in the central plateau. During the late Early–early Middle Jurassic, fan delta and alluvial fan deposits sourced from the Amdo basement to the south occurred within the Amdo suture zone, as a result of collision between the Amdo basement and Qiangtang terrane. Since the Bajocian of the Middle Jurassic, continued sea-level rise transformed the Qiangtang terrane into a south-facing shallow continental shelf, and sedimentary detritus was predominantly sourced from the Hoh Xil and Kunlun terranes to the north. The contemporaneous magmatic arc in southern Qiangtang terrane was most likely submerged in a marine setting and did not contribute much detritus to the Middle Jurassic strata. Starting from the early Late Jurassic, a depositional hiatus occurred in the southern Qiangtang terrane, whereas the shallow marine to deltaic deposition in the central Qiangtang terrane received detritus not only from the Hoh Xil and Kunlun terranes to the north, but also from the magmatic arc in southern Qiangtang terrane to the south. The arrival of abundant Jurassic arc-derived detritus in central Qiangtang terrane since ca. 163 Ma was most likely caused by the early Late Jurassic initial collision between the Lhasa and Qiangtang terranes, which raised the southern Qiangtang magmatic arc to be a source region.

INTRODUCTION

The Tibetan Plateau is a collage of terranes that was assembled during the Phanerozoic (Yin and Harrison, 2000); from south to north, they are the Himalaya, Lhasa, Qiangtang, Hoh Xil-Songpan-Ganzi (shortened to Hoh Xil hereafter), Kunlun-Qaidam, and Qilian terranes (Fig. 1A). Mesozoic tectonism, prior to the final Cenozoic India-Asia collision, contributed to the growth of the Tibetan Plateau, especially of its southern and central parts (England and Searle, 1986; Murphy et al., 1997; Kapp et al., 2005, 2007b). The collision between the Lhasa and Qiangtang terranes along the Bangong-Nujiang suture (shortened to Bangong suture hereafter; Fig. 1) is one of the most prominent tectonic events that occurred in the Mesozoic history of the Tibetan Plateau (Dewey et al., 1988; Yin and Harrison, 2000). Despite the many studies that have been conducted to understand the processes of the Lhasa-Qiangtang collision (Yin and Harrison, 2000; Zhang et al., 2012a; Zhu et al., 2013), the timing and nature of the collision remain controversial.

The current understanding of the timing and nature of the Lhasa-Qiangtang collision can be classified into two hypotheses. One of the hypotheses suggests that the collision did not occur until the early Late Cretaceous (ca. 100 Ma), based primarily on the presence of: (1) 120–108 Ma basaltic rocks with ocean island affinity within the Bangong suture zone (Zhu et al., 2006; Liu et al., 2014; Zhang et al., 2014a; Fan et al., 2015); (2) 170–140 Ma and 130–100 Ma intrusive rocks in the southern Qiangtang terrane, presumably formed by continental arc magmatism associated with the northward subduction of the Meso-Tethys oceanic lithosphere (Li et al., 2014; Hao et al., 2016; Liu et al., 2017; Liu et al., 2018); and (3) 131–121 Ma deep-marine radiolarian deposits near Gaize in the Bangong suture zone (Baxter et al., 2009). The other hypothesis suggests a diachronous collision from east in the Amdo area during the Middle–Late Jurassic (ca. 174–145 Ma; Dewey et al., 1988; Leeder et al., 1988), to west in the Shiquanhe area during the Early Cretaceous (ca. 145–110 Ma; Matte et al., 1996). This latter hypothesis is mainly based on: (1) obduction of ophiolite fragments onto the northern margin of the Lhasa terrane during the Middle–Late Jurassic near Amdo (Yin and Harrison, 2000); and (2) structural analyses that indicate major Early Cretaceous shortening in the southern Qiangtang terrane near Shiquanhe and Gaize (Kapp et al., 2005; Raterman et al., 2014).

In addition to the uncertainty in the timing of the Lhasa-Qiangtang collision, the presence of the Amdo basement, with ophiolite fragments on both its northern and southern sides (Coward et al., 1988; Fig. 1B), remains enigmatic. Yin and Harrison (2000) considered the Amdo basement as a part of the Lhasa terrane, and suggested that closure of the Meso-Tethys Ocean and collision between the Lhasa and Qiangtang terranes occurred to the north of the Amdo basement. To the contrary, Guynn et al. (2006) proposed that the Amdo basement was rifted from the Qiangtang terrane before the Early

*Current address: Géosciences Rennes, UMR–CNRS 6118, Université de Rennes 1, 35042 Rennes Cedex, France

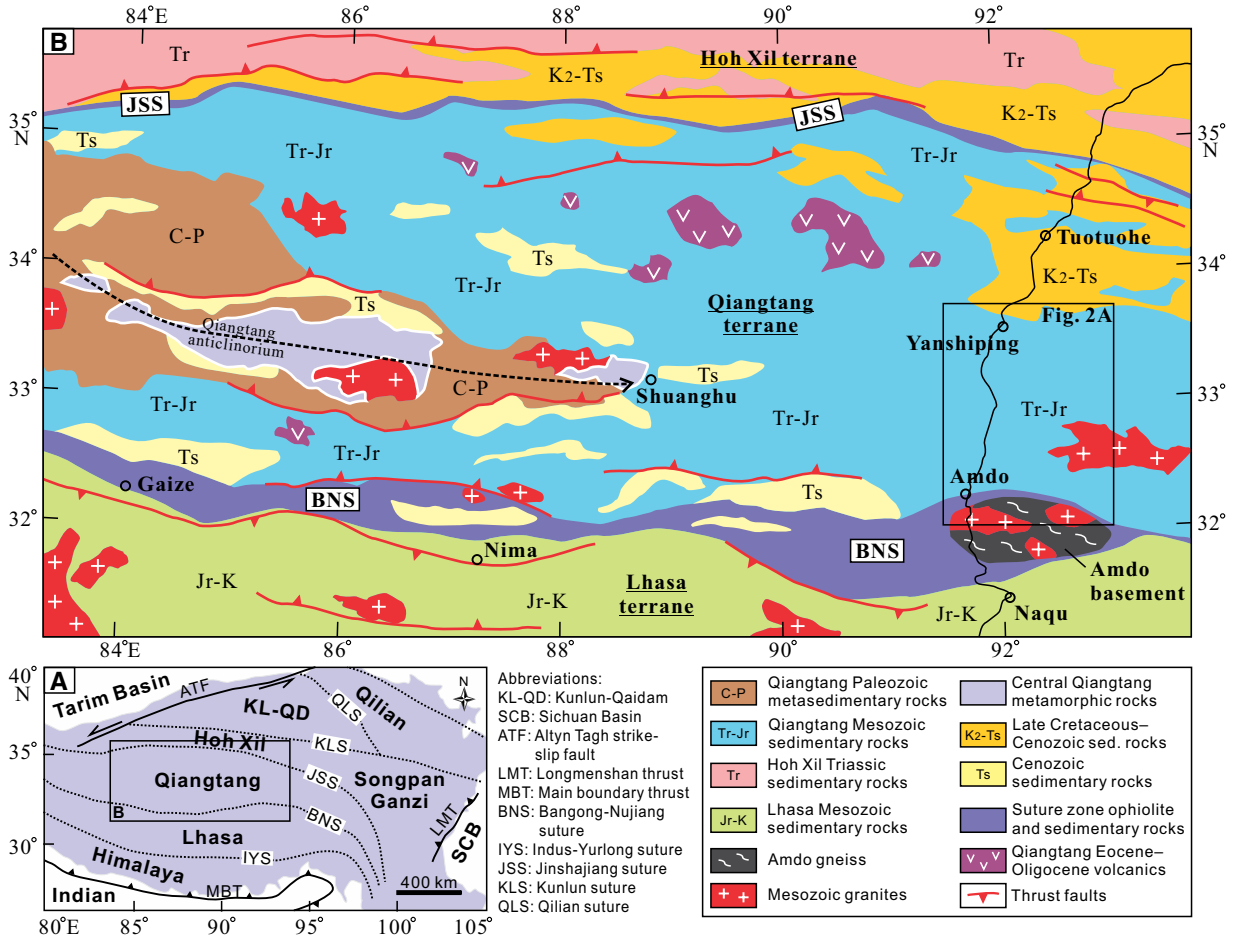

Figure 1. (A) Tibetan Plateau above the 2000 m elevation contour, showing major tectonic subdivisions and suture zones (dotted lines). Rectangular box shows location of B. (B) Simplified geologic map of the west-central Tibetan Plateau. Modified from Kapp et al. (2005). Rectangular box shows location of Fig. 2A. sed.—sedimentary.

Jurassic and then collided with the Qiangtang terrane during the Early–Middle Jurassic (ca. 190–170 Ma), which was followed by the major Lhasa-Qiangtang collision to the south of the Amdo basement.

The Qiangtang terrane holds the largest Jurassic marine deposits in the Tibetan Plateau. Previous sedimentological studies have suggested that these Jurassic strata were deposited in shallow marine to marginal marine environments (Wang et al., 2001; Wang et al., 2010a). However, the tectonic setting of these deposits is not well understood, with proposed models ranging from a retroarc foreland basin (Li et al., 2001) to a passive continental margin basin (Guo et al., 2008) to a passive rift basin (Wang et al., 2010b). Depositional environment and detrital provenance can be distinctive in different tectonic settings; e.g., a retroarc foreland basin would receive detritus mainly from the magmatic arc, whereas a passive continental margin basin would have major sediment sources from the adjacent exposed continent. This study applies the zircon U-Pb geochronology method to both sandstone and igneous samples from the Jurassic sedimentary successions in the Amdo-Yanshiping area, south-central Qiangtang terrane (Fig. 2), to infer the history of the Lhasa-Qiangtang collision and the role that the Amdo basement played during the collision. We found that: (1) the Amdo Formation received detritus mainly from the Amdo basement as a result of late Early–early Middle Jurassic collision between the Amdo basement and

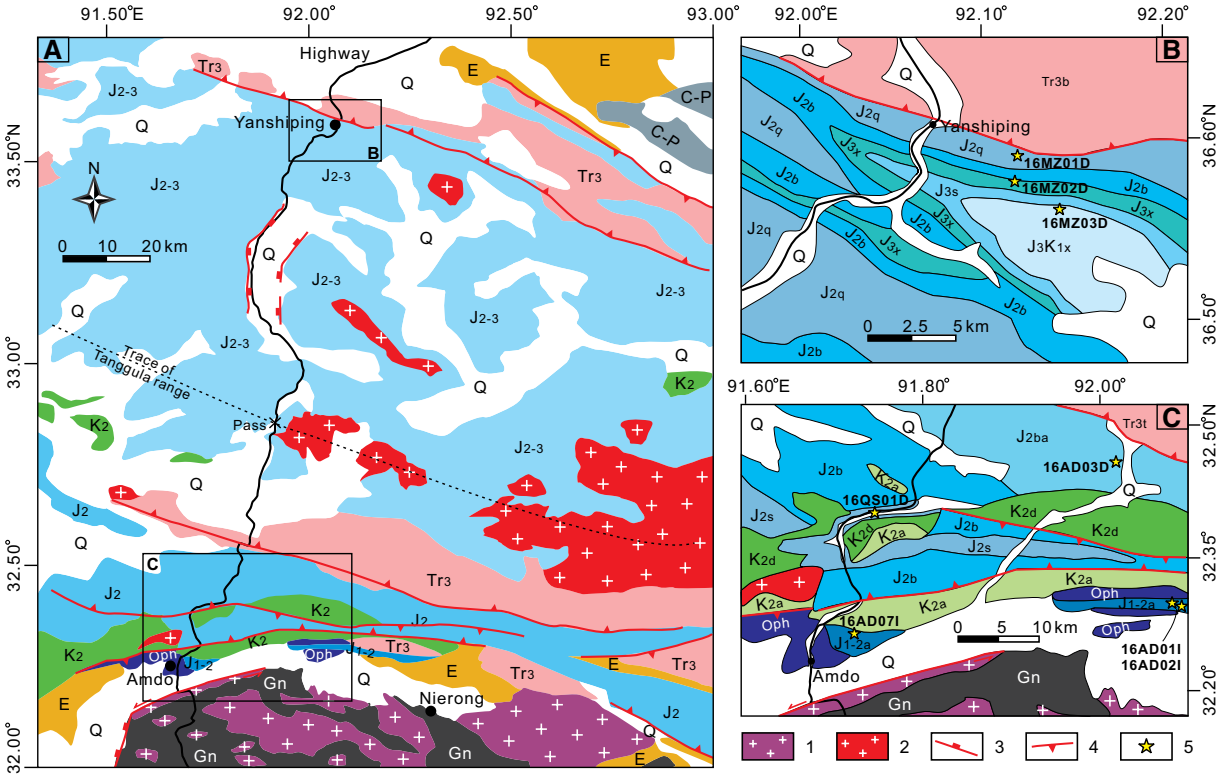

Figure 2. Geological map of the Amdo-Yanshiping region, south-central Qiangtang terrane (A), with details for the Yanshiping area (B) and Amdo area (C). Modified from Bai et al. (2005) and Li et al. (2005). Legend: 1—Early Jurassic granitoids; 2—Cretaceous granitoids; 3—normal faults; 4—reverse faults; 5—detrital zircon and igneous rock sample locations. Abbreviations: C–P—Carboniferous–Permian; Tr_3—Upper Triassic (Tr_{3b}, Bagong Formation; Tr_{3t}, Tumengela Formation); J_{1-2}—Lower–Middle Jurassic (J_{1-2a}, Amdo Formation); J_2—Middle Jurassic (J_{2b}, Buqu Formation; J_{2ba}, Bang'ai Formation; J_{2q}, Quemoco Formation; J_{2s}, Sewa Formation); J_{2-3}—Middle–Upper Jurassic; J_3—Upper Jurassic (J_{3x}, Xiali Formation; J_{3s}, Suowa Formation); J_3K_{1x}—Upper Jurassic–Lower Cretaceous Xueshan Formation; K_2—Upper Cretaceous (K_{2a}, Abushan Formation; K_{2d}, Dongqiao Formation), E—Paleogene; Q—Quaternary; Oph—ophiolite; Gn—gneiss.

Qiangtang terrane; and (2) a pronounced provenance change at ca. 163 Ma in the central Qiangtang terrane was most likely caused by the early Late Jurassic initial collision between the Lhasa and Qiangtang terranes. This study highlights the complex processes of terrane accretions in the Mesozoic history of Tibet.

GEOLOGIC SETTING

Qiangtang Terrane

The Qiangtang terrane, located in the central Tibetan Plateau, is separated from the Hoh Xil-Songpan-Ganzi terrane to the north by the Jinsha suture, and the Lhasa terrane to the south by the Bangong-Nujiang suture (Fig. 1). During Carboniferous–Permian time, the Qiangtang and Lhasa terranes were located in the Southern Hemisphere on the northern margin of Gondwana, which was separated from Laurasia in the Northern Hemisphere by the Paleo-Tethys Ocean (Gehrels et al., 2011). The Qiangtang terrane had drifted toward Laurasia by the Late Permian, giving birth to the Meso-Tethys Ocean (Metcalfe, 1996). The terrane eventually collided with Laurasia along the Jinsha suture, which led to the closure of the Paleo-Tethys Ocean during Late Triassic to Early Jurassic time. During the Middle–Late Jurassic, extensive siliciclastic and carbonate rocks were deposited in shallow and marginal marine environments on the Qiangtang terrane (Wang et al., 2001). After a depositional hiatus during the Early Cretaceous, the Late Cretaceous and Cenozoic deposition on

the Qiangtang terrane consisted of primarily terrestrial intermontane clastic rocks (Wang and Pan, 2012).

In the central western Qiangtang terrane, Carboniferous–Permian strata are exposed in the Qiangtang anticlinorium (Yin and Harrison, 2000), whose core region is characterized by a belt of high-pressure metamorphic rocks (Li et al., 1995; Kapp et al., 2000; Zhang et al., 2006a). Some researchers have proposed that the metamorphic belt represents an early Mesozoic suture zone that separates the east Qiangtang subterrane from the west Qiangtang subterrane (Li et al., 1995; Zhang et al., 2006a, 2006b), while others proposed that the metamorphic belt is an underthrusted early Mesozoic mélange belt, formed during the southward subduction of the Paleo-Tethys oceanic lithosphere beneath the Qiangtang terrane (Kapp et al., 2003; Pullen et al., 2008).

Bangong Suture and Amdo Basement

The Bangong suture was formed by closure of the Meso-Tethys Ocean basin and collision between the Lhasa and Qiangtang terranes (Dewey et al., 1988). Primary components in the suture zone include deep-marine flysch rocks, mélanges, volcanics, and ophiolite fragments (Wang and Pan, 2012). Ophiolite rocks exposed discontinuously in the suture zone were formed during the Late Triassic to Early Jurassic and were obducted southward onto the northern margin of the Lhasa terrane during the Middle–Late Jurassic (Leeder et al., 1988; Matte et al., 1996). Marine sedimentation in the suture zone, however, may have continued until the middle Early Cretaceous (Kapp et al., 2007a; Baxter et al., 2009; Li et al., 2017).

Between Amdo and Naqu, the Bangong suture zone is divided by the Amdo basement into two branches (Fig. 1B); the northern branch is named the Amdo suture hereafter. The Amdo basement is characterized by Early Jurassic granitoids (185–170 Ma) and high-grade granitic orthogneisses and paragneisses (Guynn et al., 2006, 2012; Zhang et al., 2012b). Different views exist concerning formation of the Early Jurassic metamorphism. Some researchers consider that the metamorphism was caused by deep subduction during the collision between the Amdo basement and Qiangtang terrane (Zhang et al., 2012b; Zhang et al., 2014c). Others consider the metamorphism to have been related to the development of a continental arc associated with the northward subduction of the Meso-Tethys oceanic lithosphere beneath the Amdo basement (Guynn et al., 2006).

Jurassic Stratigraphy and Age Constraints in the Amdo-Yanshiping Region

The Amdo-Yanshiping region is located along the Golmud-Lhasa highway in the south-central Qiangtang terrane (Fig. 1B). The region is bounded by the Amdo basement to the south and the Late Cretaceous–Cenozoic Hoh Xil basin to the north. With the Tanggula range as a divide, the region can be divided into the Amdo area on the south and the Yanshiping area on the north (Fig. 2A). The Mesozoic stratigraphic successions are different in these two areas (Figs. 3 and 4).

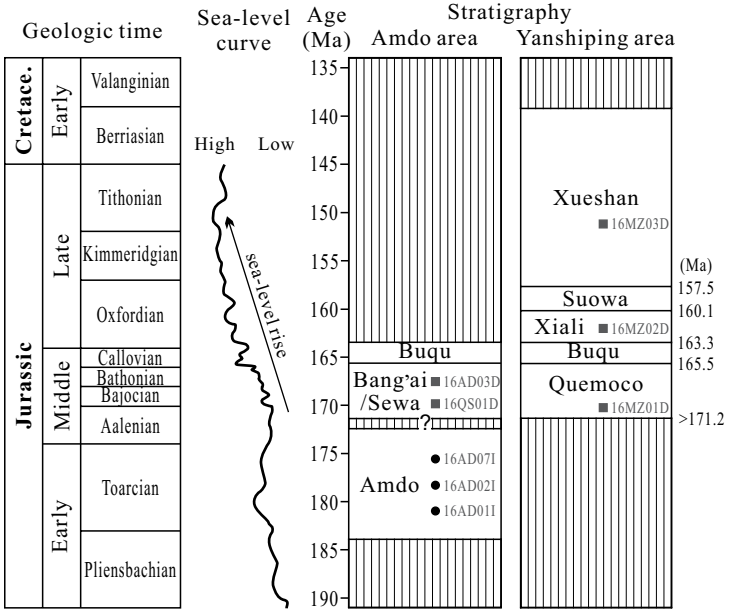

Figure 3. Stratigraphy in the Amdo-Yanshiping area, south-central Qiangtang terrane, summarized from Bai et al. (2005) and Li et al. (2005). Also shown are the Jurassic sea-level curve, highlighting significant sea-level rise during the Middle–Late Jurassic (Hallam, 1988); and stratigraphic heights of geochronologic samples (squares, detrital zircon samples; circles, igneous rocks). Vertical bars indicate depositional hiatus. Age constraints in the Yanshiping area are from Fang et al. (2016). Cretace.—Cretaceous.

The Jurassic depositional succession in the Amdo area includes the Amdo, Sewa, Bang'ai, and Buqu formations (Fig. 3). The Amdo Formation was previously considered Late Jurassic in age (Sun, 2005). However, our new zircon U-Pb ages from an interlayered tuff bed indicates deposition as early as the late Early Jurassic (Fig. 3; see Chronostratigraphy section for details). The Sewa and Buqu formations are Middle Jurassic in age based on marine fossils (Bai et al., 2005; Yin, 2005) and stratigraphic correlations with strata in the Yanshiping area. The Bang'ai Formation was previously assigned a Late Jurassic–Early Cretaceous age (Sun, 2005). Our new detrital zircon U-Pb age data place the formation in the Middle Jurassic, an equivalent of the Sewa Formation (Fig. 3; see Chronostratigraphy section for details).

The depositional succession in the Yanshiping area is known as the Yanshiping Group, which includes the Quemoco, Buqu, Xiali, Suowa, and Xueshan formations, from oldest to youngest (Fig. 3). Abundant marine fossils, including bivalves, brachiopods, and ammonoids, indicate that the Yanshiping Group was deposited during the Middle and Late Jurassic (Yin, 1987; Yang and Yin,

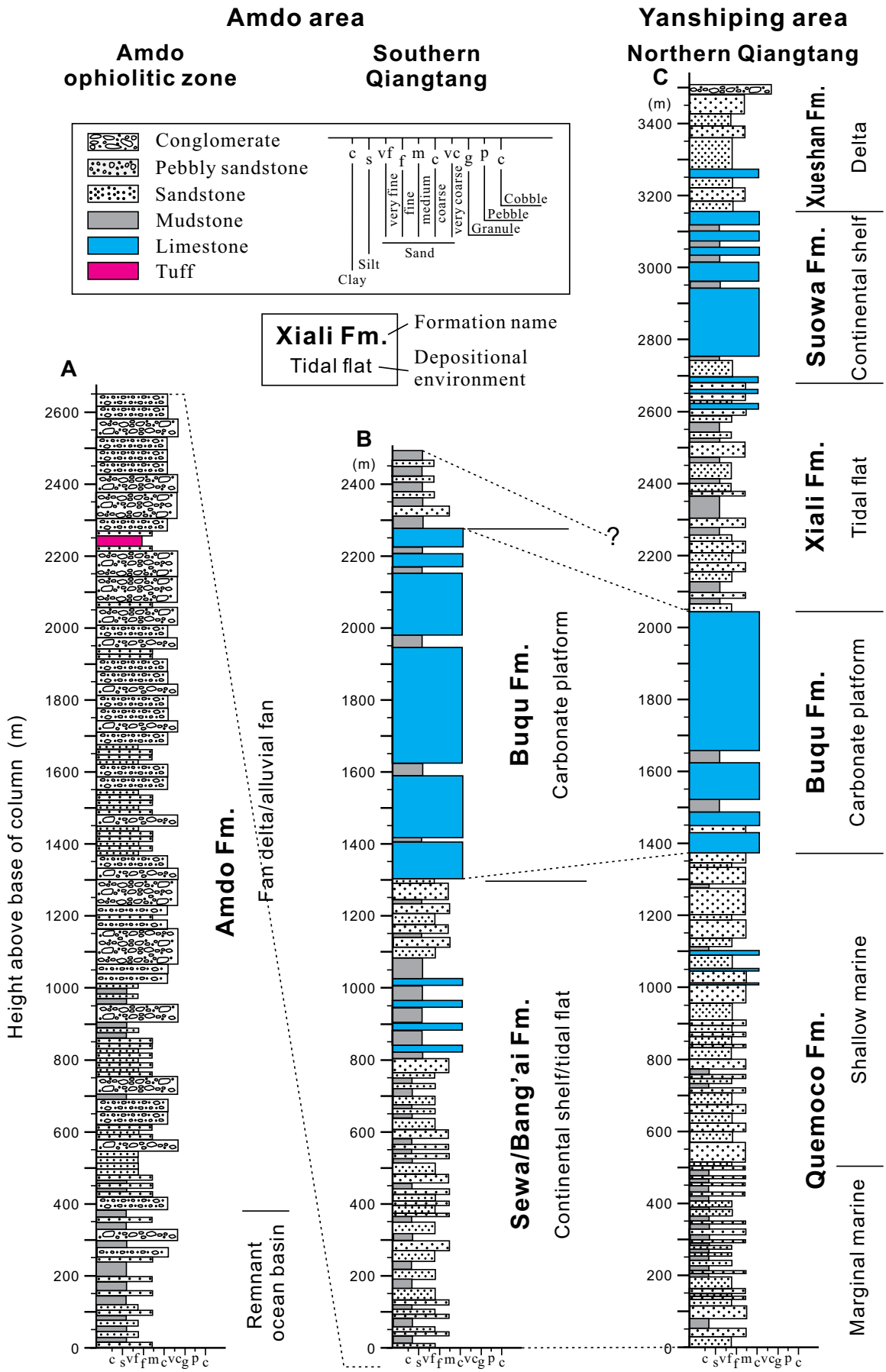

Figure 4. Summary of lithostratigraphy in the Amdo (A–B) and Yanshiping (C) areas; also shown are the interpreted depositional environments of different formations. Based on Fang et al. (2016), Yao et al. (2011), Sun (2005), and this study.

1988; Bai, 1989; Yao et al., 2011). Recent magnetostratigraphic studies refine the depositional ages of these five formations to >171.2–165.5 Ma, 165.5–163.3 Ma, 163.3–160.1 Ma, 160.1–157.5 Ma, and <157.5 Ma, respectively (Fig. 3; Fang et al., 2016; Song et al., 2016). Although some researchers suggest that the Xueshan Formation is only Late Jurassic in age, others argue that it extends into the Early Cretaceous Berriasian Age (ca. 140 Ma; BGMRQH, 1997; Li and Batten, 2004; Li et al., 2011).

STRATIGRAPHY

Jurassic stratigraphy in the study area has been measured and described in numerous previous studies (Yang and Yin, 1988; Bai, 1989; BGMRQH, 1997; Wang et al., 2001; Sun, 2005; Yao et al., 2011; Fang et al., 2016). Here we add detailed description of the lithofacies and summarize fossils and interpretation of depositional environments from the literature and our own observation.

Amdo Area

In the Amdo area, in addition to shallow marine siliciclastic and carbonate rocks (Fig. 4B) that are similar to those in the Yanshiping area (Fig. 4C), there are also limited outcrops of conglomerate beds with fan delta and alluvial fan origins (Fig. 4A).

The Amdo Formation crops out only within the Amdo ophiolitic zone between the southern Qiangtang terrane and Amdo basement (Fig. 2C). The formation is >2600 m thick near Amdo (Sun, 2005). Its basal part contains predominantly interbedded mudstone and thinly to medium-bedded, fine-grained sandstone and minor amounts of pebbly sandstone and conglomerate (Fig. 4A). The sandstone units have normal grading and planar laminations (Fig. 5A), and the mudstone units have pelagic to hemipelagic trace fossils (Sun, 2005). The basal part was inferred to have been deposited in a remnant deep-marine basin (Sun, 2005).

The remaining majority of the Amdo Formation consists of thinly to thickly bedded conglomerate and sandstone (Fig. 4A) with scour surfaces and large-scale planar cross-bedding. The conglomerate beds are poorly sorted and mostly clast supported, with some clasts >1 m in diameter. The clasts include limestone, chert, and andesite in the lower part (Fig. 5B), whereas they are dominated by dacite, rhyolite, and granodiorite in the upper part. Most of the conglomerate beds are massive, but some show weak imbrication and crude stratification. Several layers of dacite and rhyolite tuff (Fig. 5C), as thick as a few tens of meters, were found in the formation. The lower and middle part of the Amdo Formation most likely reflects a fan delta setting, whereas the upper part includes both alluvial fan and braided river facies (Sun, 2005).

Both the Sewa and Bang'ai formations contain interbedded mudstone, fine-grained sandstone, and limestone (Fig. 4B). The limestone beds are dark gray or black, are medium to thickly bedded, and contain marine bivalves and corals (Sun, 2005). The mudstone and sandstone beds are dark brown or gray and are thinly to medium bedded (Fig. 5D). These formations contain abundant sedimentary structures, such as lenticular bedding, wavy bedding, flaser bedding, and herringbone cross-stratification (Sun, 2005). It is most likely that these two formations were deposited in a shallow marine environment, but with frequent tidal influence.

The Buqu Formation consists predominantly of massive, thickly bedded carbonate and minor amounts of mudstone and sandstone (Fig. 4B; Bai et al., 2005). Marine bivalves, brachiopods, and ammonoids have been reported (Bai et al., 2005; Yin, 2005). The Buqu Formation was deposited in a continental shelf carbonate platform environment.

Yanshiping Area

In the Yanshiping area, the Middle and Upper Jurassic marine strata of the Yanshiping Group unconformably overlie Upper Triassic rocks (Fig. 2B). The five subdivided formations are conformable with each other (Fig. 3) and exhibit formation-scale sandstone-carbonate cycles (Fig. 4C; Wang et al., 2001).

The Quemoco Formation is ~1400 m thick (Fig. 4C). Its lower part consists dominantly of dark-brown or dark-gray mudstone, with a minor amount of dark-brown sandstone (Fig. 5E), gypsum, and weakly developed paleosols. Mud cracks, tracks, burrows, and plant debris are common in the mudstone units (Fang et al., 2016), whereas planar cross-bedding, scour surfaces, ripple marks, and water-escape structures are commonly observed in the sandstone. Both fresh- and brackish-water bivalves are present (Bai, 1989; Fang et al., 2016). The lower Quemoco Formation was probably deposited in a marginal marine to fluvial depositional environment (Yao et al., 2011). The upper part of the formation contains mainly dark-brown and dark-gray sandstone and siltstone, interbedded with minor amounts of mudstone and limestone. The sandstone beds are massive with sharp bases. Coarsening-upward sequences are common. Bivalves found in this part are exclusively brackish and marine species (Bai, 1989; Fang et al., 2016). The upper Quemoco Formation was probably deposited in a shallow marine inner shelf environment (Yao et al., 2011) that periodically shoaled to a brackish lagoon environment.

The Buqu Formation is an ~600-m-thick carbonate succession (Fig. 4C) that consists mainly of gray, medium- to thickly bedded, massive or laminated limestone. Some sandstone beds occur in the lower part. Marine fossils including bivalves, brachiopods, ammonoids, and foraminifera are abundant (Bai, 1989; Yao et al., 2011). The Buqu Formation was deposited in a shallow marine carbonate platform environment (Yao et al., 2011; Fang et al., 2016).

The Xiali Formation is ~600 m thick and contains brown, gray, and green sandstone that fines upward to mudstone (Fig. 4C). Minor limestone and gypsum layers are present in the upper part. The sandstone units are medium to thickly bedded and mostly massive. Sandstone beds show planar laminations, ripple marks, flaser bedding (Fig. 5F), wavy bedding, lenticular bedding, and herringbone cross-stratification. Storm-related depositional successions have

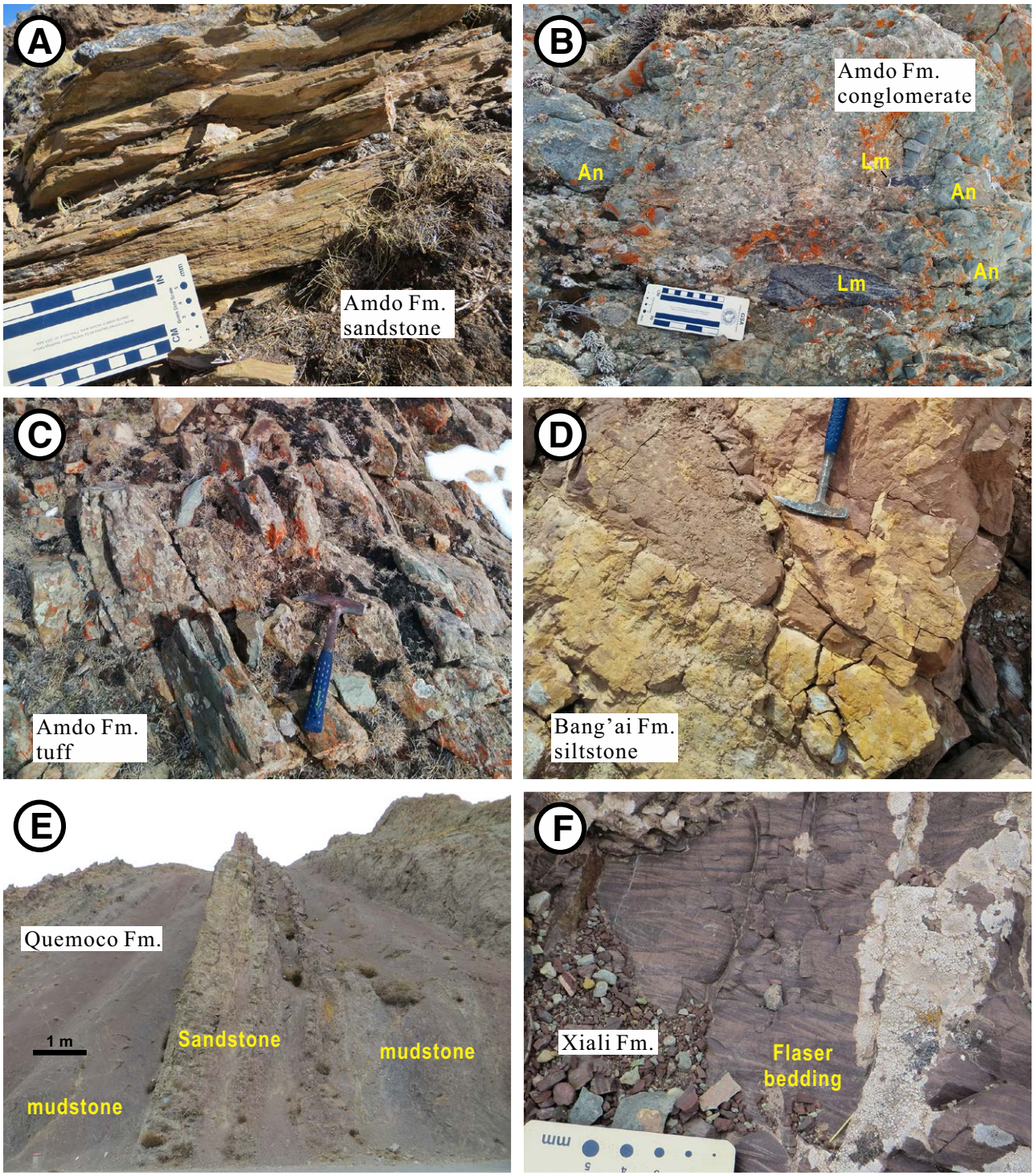

Figure 5. Field photos of lithofacies in the Amdo-Yanshiping area. (A) Fine-grained sandstone with planar bedding in the lower Amdo Formation, Amdo area. Interpreted as fan delta environment. (B) Conglomerate of the Amdo Formation, Amdo area. Clasts are dominated by limestone (Lm) and andesite (An). Interpreted as alluvial fan environment. (C) Layered tuff of the Amdo Formation, Amdo area. (D) Massive siltstone of the Bang'ai Formation, Amdo area. Interpreted as continental shelf environment. (E) Interbedded sandstone and mudstone of the lower Quemoco Formation, Yanshiping area. Interpreted as delta environment. (F) Sandstone with flaser bedding in the Xiali Formation, Yanshiping area. Interpreted as tidal environment.

also been reported (Yao et al., 2011). The mudstone units are thinly bedded and contain mud cracks and trace fossils. Marine bivalve fossils are abundant (Bai, 1989; Fang et al., 2016). This formation was mostly likely deposited in a marginal marine environment, dominantly within a tidal flat setting (Yao et al., 2011; Fang et al., 2016).

The Suowa Formation is ~450 m thick (Fig. 4C) and contains interbedded gray limestone and mudstone. Limestone is medium to thickly bedded and mainly includes micrite and sparse biomicrite (BGMRQH, 1997). Bivalves and brachiopods are the most abundant fossils, while ammonoids and crinoid stems have also been reported (Bai, 1989; Fang et al., 2016). The Suowa Formation was probably deposited in a carbonate ramp environment (Yao et al., 2011; Fang et al., 2016).

The Xueshan Formation contains interbedded gray, green, and dark-brown thinly bedded sandstone and mudstone (Fig. 4C). Minor bioclastic limestone beds occur in the lower part, whereas minor conglomerate and pebbly sandstone beds showing planar cross-stratification and scour surfaces occur in the upper part (Yao et al., 2011; Fang et al., 2016). Bivalves discovered in the lower part are exclusively of marine to brackish-water origin (Yang and Yin, 1988; Bai, 1989); in contrast, both fresh- and brackish-water bivalves, along with plant debris and pollen, are present in the upper part (Yang and Yin, 1988; Bai, 1989; Yao et al., 2011). It is inferred that the lower Xueshan Formation was deposited in a marginal marine environment, which transitioned to a continental depositional environment, most likely fluvial, in the upper part (Yao et al., 2011; Fang et al., 2016).

METHODS

Five sandstone and three igneous samples were collected in the field after removing the weathered surface layers. Three of the sandstone samples were collected from the Yanshiping area and two from the Amdo area (Figs. 2 and 3). All three igneous rocks were collected from the Amdo Formation, and include one interlayered tuff, one andesite clast, and one granite clast.

Following crushing and grinding of the rock samples, zircons were separated and concentrated using a Wilfley table, a Frantz magnetic separator, and heavy liquids (Gehrels et al., 2006). Zircon U-Pb dating was carried out at the Arizona LaserChron center at the University of Arizona (Tucson, Arizona, USA) using a Thermo Element 2 single collector inductively coupled plasma–mass spectrometer coupled to a Photon Machines Analyte G2 excimer laser. Detailed analysis methods follow Pullen et al. (2014). Common Pb corrections were made using the measured ^{204}Pb and assuming an initial Pb composition from Stacey and Kramers (1975). Sri Lankan and FC-1 zircon standards were used to correct for isotope fractionation, and the R33 zircon standard was treated as an unknown and used to monitor the fractionation correction. More than 200 grains were analyzed for each sandstone sample and >30 grains for each igneous sample.

Reported uncertainties include measurement errors at the 1σ level. For ^{206}Pb/^{238}U ages, analyses with >10% uncertainty are not included; for ^{206}Pb/^{207}Pb ages, analyses with >10% uncertainty are not included unless the ^{206}Pb/^{238}U ages are <400 Ma. Concordance is not reported for ^{206}Pb/^{238}U ages <400 Ma because of large uncertainty in ^{206}Pb/^{207}Pb ages. For ages >400 Ma, only analyses with <30% discordance and <5% reverse discordance are included. The used ages are ^{206}Pb/^{238}U ages for grains with ages <900 Ma and ^{206}Pb/^{207}Pb ages for grains with ages >900 Ma. After filtering the data, our analysis yields >1200 new zircon ages. All of the zircon U-Pb age data are presented in Table S1 in the Supplemental Files[1].

SEDIMENT PROVENANCE

Potential Source Terranes

Potential sediment source regions for the Jurassic rocks in the study area include: Amdo basement and late Paleozoic–early Mesozoic rocks in the Lhasa terrane to the south; and Triassic and older rocks in the Kunlun and Hoh Xil terranes to the north (Fig. 1B). In addition, the late Paleozoic metasedimentary and metamorphic rocks in the central-western Qiangtang terrane could also have been exhumed to provide detritus while the remaining majority of the Qiangtang terrane was below sea level to receive marine deposition during the Middle–Late Jurassic (Fig. 1B).

The northern and southern Lhasa terranes are dominated by Jurassic–Cretaceous sedimentary rocks and Cretaceous–Cenozoic magmatic rocks, respectively (Zhu et al., 2013). Pre-Jurassic rocks crop out mainly in the central Lhasa terrane (Zhu et al., 2013). The detrital zircon age spectrum of these pre-Jurassic rocks has two major age clusters of 500–650 Ma and 1050–1250 Ma (Fig. 6A), and a few minor ones (Leier et al., 2007; Gehrels et al., 2011; Zhu et al., 2011; Cai et al., 2016).

The Amdo basement contains two major lithologic units, including the Early Jurassic granitoids of 170–185 Ma (Fig. 6B; Guynn et al., 2006) and the Neoproterozoic and Cambrian orthogneisses of 820–920 Ma and 460–540 Ma (Guynn et al., 2012). There is also limited presence of lower Paleozoic metasedimentary rocks with age clusters of 450–550 Ma, 750–850 Ma, 850–1000 Ma, and 2400–2600 Ma (Fig. 6B; Guynn et al., 2012).

The central-western Qiangtang terrane is characterized by Carboniferous–Permian metasedimentary and Triassic high-pressure metamorphic rocks (Fig. 1B). The detrital zircon age spectrum of these rocks has three major age clusters of 500–700 Ma, 700–900 Ma, and 900–1000 Ma (Fig. 6C; Pullen et al., 2008, 2011; Gehrels et al., 2011). Adjacent to these upper Paleozoic rocks, Triassic granitoids of 200–230 Ma are present locally (Zhang et al., 2014b; Li et al., 2015). Jurassic (170–140 Ma) and Early Cretaceous (130–100 Ma) igneous rocks are exposed in the southern Qiangtang terrane (Fig. 6C; Li et al., 2014; Liu et al., 2017; Hao et al., 2016, and references therein).

In the Hoh Xil terrane, exposed pre-Jurassic rocks are nearly exclusively Triassic deep-marine clastic rocks. Their detrital zircon signatures are characterized by two major age clusters of 200–350 Ma and 400–500 Ma, and two

Table S1. Zircon U-Pb geochronology data for all sandstone and igneous samples from the Amdo-

Analysis	U (ppm)	I^#5% I^05%	&'()	I^#5%* I^,5%*	+ 123	I^,5%* I45&*	+ 123	I^#5%* I46&	+ 123	-./. 7/.8
16MZ01D; coarse-grained sandstone; Quemoco Formation, Yanshiping area; 33.5803°N, 92.1286°										
16MZ01D Spot 214	452	17133	1.3	19.2622	2.3	0.2012	4.4	0.0281	3.8	0.86
16MZ01D Spot 122	884	46540	2.5	19.3452	1.3	0.2187	3.2	0.0307	2.9	0.91
16MZ01D Spot 1	338	141158	3.4	19.2061	1.2	0.2238	4.1	0.0312	3.9	0.95
16MZ01D Spot 121	100	5849	3.6	20.0038	1.8	0.2157	3.6	0.0313	3.1	0.86
16MZ01D Spot 118	594	20846	2.5	19.2668	1.0	0.2334	3.0	0.0326	2.9	0.94
16MZ01D Spot 196	899	36065	4.1	19.5795	1.4	0.2349	3.5	0.0334	3.1	0.91
16MZ01D Spot 157	713	110114	1.7	19.5527	1.4	0.2515	3.4	0.0357	3.1	0.92
16MZ01D Spot 77	311	6279	2.5	18.6446	1.8	0.2660	4.0	0.0360	3.6	0.90
16MZ01D Spot 146	177	21925	2.6	19.0607	1.9	0.2630	3.3	0.0364	2.7	0.82
16MZ01D Spot 220	922	4936	2.4	17.8634	1.6	0.2875	3.1	0.0373	2.6	0.85
16MZ01D Spot 87	547	4146	1.5	20.2011	2.1	0.2599	3.8	0.0375	3.2	0.84
16MZ01D Spot 128	482	20582	1.7	19.1451	1.3	0.2712	3.4	0.0377	3.2	0.93
16MZ01D Spot 19	679	11263	1.6	18.1184	1.7	0.2890	3.6	0.0380	3.2	0.89
16MZ01D Spot 91	1227	60643	2.0	19.3929	1.0	0.2774	2.7	0.0390	2.5	0.93
16MZ01D Spot 142	462	9055	1.9	19.5300	1.7	0.2784	3.5	0.0395	3.0	0.87
16MZ01D Spot 101	399	17230	1.4	19.5145	1.1	0.2798	2.4	0.0396	2.1	0.89
16MZ01D Spot 184	214	419013	1.2	18.2822	1.8	0.3003	3.1	0.0398	2.6	0.83
16MZ01D Spot 96	436	6693	1.3	19.6412	1.5	0.2810	3.0	0.0400	2.6	0.87
16MZ01D Spot 15	250	85847	1.7	18.9906	1.4	0.2946	3.1	0.0406	2.7	0.88
16MZ01D Spot 202	1683	49195	2.4	19.2665	1.0	0.3001	2.5	0.0420	2.3	0.91
16MZ01D Spot 40	347	11169	0.8	12.2874	4.1	0.4730	5.0	0.0422	2.8	0.57
16MZ01D Spot 143	262	34666	2.6	18.8730	1.3	0.3112	3.1	0.0426	2.8	0.91
16MZ01D Spot 89	539	30189	1.2	18.8356	1.2	0.3127	3.6	0.0427	3.4	0.95
16MZ01D Spot 63	186	105676	2.0	18.6196	1.6	0.3231	3.6	0.0437	3.3	0.90
16MZ01D Spot 99	349	2233	1.9	20.9878	7.1	0.2983	7.6	0.0454	2.8	0.37
16MZ01D Spot 162	433	11591	2.1	18.5556	1.6	0.3381	4.4	0.0455	4.1	0.93
16MZ01D Spot 26	233	7607	1.7	19.8609	1.7	0.3241	2.8	0.0467	2.3	0.81
16MZ01D Spot 60	399	4686	1.1	19.9207	2.2	0.3308	3.6	0.0478	2.8	0.79
16MZ01D Spot 192	245	36387	1.6	17.5319	1.1	0.3848	2.7	0.0489	2.4	0.90
16MZ01D Spot 24	594	28997	1.0	18.3882	1.3	0.3683	3.2	0.0491	2.9	0.91
16MZ01D Spot 120	784	14720	1.8	18.4163	1.2	0.3709	3.5	0.0496	3.3	0.94
16MZ01D Spot 153	546	20037	1.1	18.6859	0.9	0.3833	3.5	0.0520	3.4	0.97
16MZ01D Spot 147	273	4062	2.1	19.7353	2.8	0.3655	4.6	0.0523	3.6	0.79
16MZ01D Spot 97	136	9079	1.9	18.4319	1.8	0.4034	3.1	0.0539	2.5	0.81
16MZ01D Spot 46	417	21028	4.2	18.8133	1.2	0.3980	3.0	0.0543	2.7	0.92
16MZ01D Spot 198	218	5275	1.2	19.3671	1.5	0.3874	3.1	0.0544	2.7	0.88
16MZ01D Spot 21	653	24280	1.9	18.8507	1.3	0.4035	3.7	0.0552	3.4	0.93

[1]Supplemental Files. Table S1: Detrital zircon and igneous rock U-Pb ages. Figure S1: Detrital zircon histograms. Figure S2: Amdo Formation sandstone quartz-feldspar-lithics diagram. Please visit https://doi.org/10.1130/GES01649.S1 or access the full-text article on www.gsapubs.org to view the Supplemental Files.

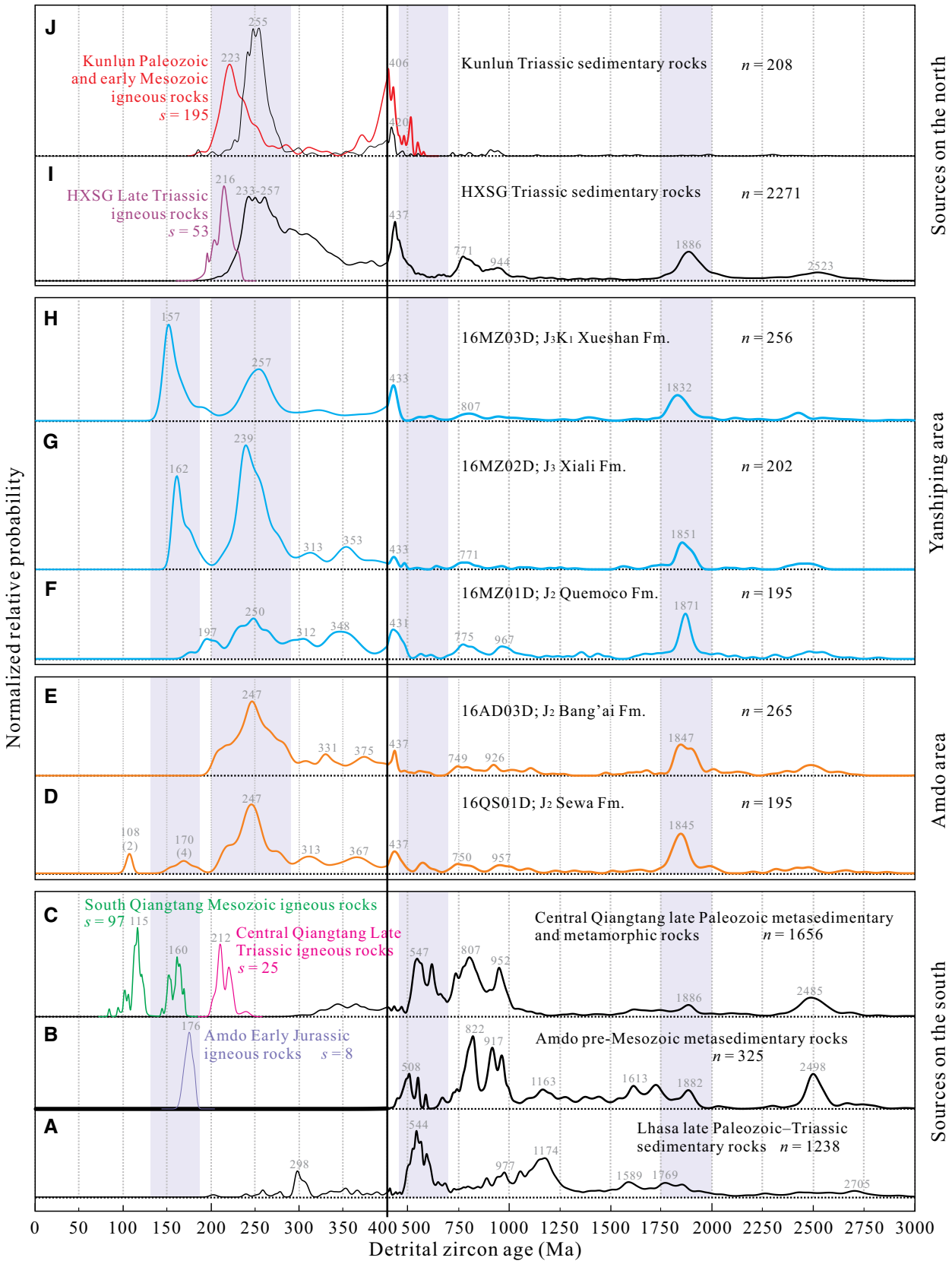

Figure 6. Normalized relative probability plots for rocks in potential source regions (A–C and I–J; see text for references) and newly collected sandstone samples from the Amdo (D–E) and Yanshiping (F–H) areas. Vertical bands highlight age ranges of 140–190 Ma, 200–290 Ma, 450–650 Ma, and 1750–2000 Ma. Refer to Figure 2 for unit symbols. *n*—numbers of detrital zircon grains analyzed for each sandstone sample; *s*—numbers of magmatic samples analyzed. Note the horizontal scale difference between 0–400 Ma and 400–3000 Ma. HXSG—Hoh Xil–Songpan–Ganzi; Fm.—Formation.

minor clusters of 700–1000 Ma and 1800–2000 Ma (Fig. 6I; Ding et al., 2013). The limitedly exposed Triassic rocks in the Qiangtang terrane have a similar age spectrum as the Hoh Xil Triassic rocks. There are also sporadic exposures of Late Triassic granitoids that have zircon U-Pb ages of 195–230 Ma (Fig. 6I; see summary in Zhang et al., 2014b).

Rocks in the Kunlun terrane can be classified into two groups: (1) Triassic sedimentary rocks, with a prominent age cluster between 200 and 300 Ma and a minor cluster between 380 and 450 Ma (Fig. 6J; Ding et al., 2013); and (2) middle Paleozoic and early Mesozoic granitoids that range from 350 to 450 Ma and from 200 to 250 Ma, respectively (Fig. 6J; see summary in Cheng et al., 2016).

New Geochronology Data and Provenance Interpretations

Yanshiping Area

Sandstone sample 16MZ01D from the Quemoco Formation (Figs. 2B and 3) yields 195 usable ages (Fig. 6F; see Fig. S1 for histogram [footnote 1]). There are two major age clusters of 195–500 Ma and 1800–2000 Ma that account for 56% of the population. The remaining grains fall in 700–900 Ma, 900–1050 Ma, and a few other insignificant age clusters.

Sandstone samples 16MZ02D and 16MZ03D are from the Xiali and Xueshan formations (Figs. 2B and 3) and yield 202 and 256 usable ages, respectively (Figs. 6G–6H). These two samples have very similar age spectra (Fig. 7), including three prominent age clusters of 150–200 Ma, 200–300 Ma, and 1800–2000 Ma. Compared with 16MZ02D, sample 16MZ03D has an additional age cluster of 390–450 Ma. The remaining age clusters are all statistically insignificant. The youngest cluster of ages yields a maximum depositional age of 162.3 (+1.9/–2.0) Ma (n = 16, TuffZirc age, which is the median age of the largest cluster of at least five ranked analyses of the youngest group with 1σ uncertainty; Ludwig and Mundil, 2002) and 154.9 (+6.8/–1.6) Ma (n = 36, TuffZirc age) for the Xiali and Xueshan formations, respectively. These maximum depositional ages agree with their magnetostratigraphic ages, which are 163.3–160.1 Ma and <157.5 Ma, respectively (Fig. 3; Fang et al., 2016).

All the three detrital zircon samples have two major age clusters of 200–300 Ma and 1800–2000 Ma, and insignificant clusters between 500 and 1000 Ma. These features are similar to those of the Hoh Xil Triassic sedimentary rocks (Fig. 6I), suggesting sediment recycling from the Triassic rocks to the north during Jurassic time. We cannot completely rule out the possibility of detrital contribution from the Kunlun terrane (Fig. 6J) despite that this source lacks the 1800–2000 Ma age cluster. The central Qiangtang late Paleozoic metasedimentary and metamorphic rocks might have contributed detritus to the Jurassic deposits in the southwestern Qiangtang terrane (Huang et al., 2016; Li et al., 2017), but we did not observe their zircon age signals in the Amdo-Yanshiping samples.

Compared to the sample from the Quemoco Formation (Fig. 6F), the two samples from the Xiali and Xueshan formations both have a strong age cluster of Jurassic zircons (150–200 Ma; Figs. 6G–6H). This cluster matches only the timing of continental arc magmatism in the southern Qiangtang terrane (Fig. 6C; Li et al., 2014; Hao et al., 2016; Liu et al., 2017), suggesting that erosion of the magmatic arc provided abundant detritus to the Xiali and Xueshan depositions. This interpretation is supported by the observation of abundant feldspar and volcanic rock fragments in thin sections of these two formations (Fig. 8A). The lack of Jurassic zircon grains in the Quemoco Formation suggests either that sediment routing was different and thus arc-derived sediments were not transported to this region, or that the arc was a submarine feature during the Middle Jurassic, or both.

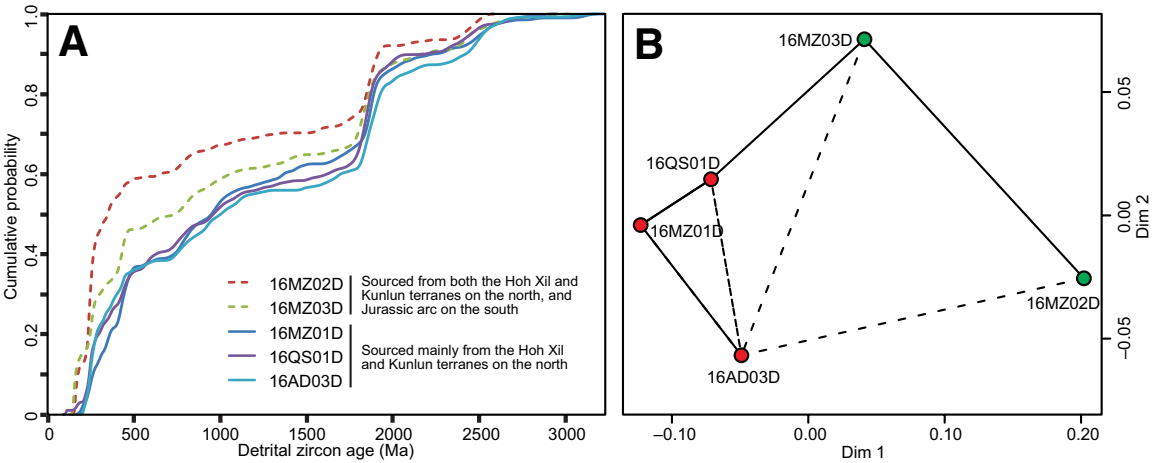

Figure 7. Cumulative probability plot (A) and classical nonmetric multidimensional scaling (MDS) plot (B) of the sandstone detrital zircon samples from the Amdo and Yanshiping areas. For the cumulative probability plot, plots of similar shape share similar provenance. For the MDS plot, the closer two samples are, the more similarity they share in zircon age spectra. The solid and dashed lines are nearest neighbor lines, whereas the dashed lines indicate a weaker relationship (Vermeesch et al., 2016). Dim 1 and Dim 2 are dimensionless axes. Note that both plots show similarities between samples 16MZ02D and 16MZ03D, as well as between samples 16QS01D, 16AD03D and 16MZ01D.

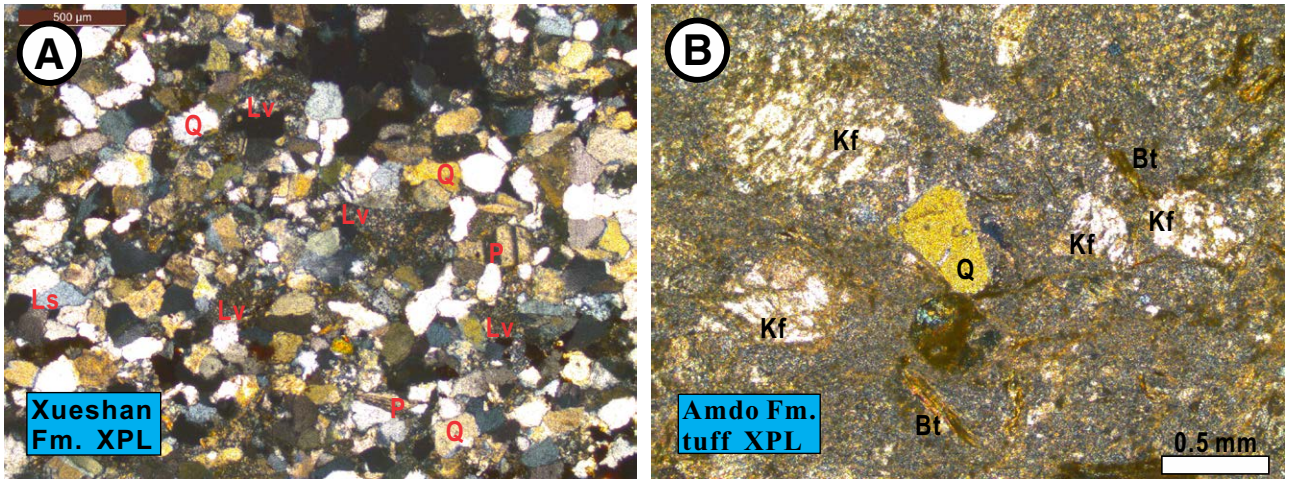

Figure 8. Photographs of petrographic thin sections under cross polarized light (XPL). (A) Sandstone sample in the Xueshan Formation showing framework grains dominated by quartz (Q), volcanic lithics (Lv), sedimentary lithics (Ls), and plagioclase (P). (B) Tuff sample in the Amdo Formation (Q—quartz; Bt—biotite; Kf—potassium feldspar).

Amdo Area

Sandstone samples 16QS01D and 16AD03D are from the Sewa and Bang'ai formations (Figs. 2C and 3) and yield 195 and 265 usable ages, respectively (Figs. 6D–6E). The age clusters of these two samples are nearly identical. Both of them have two prominent age clusters of 205–305 Ma and 1800–2000 Ma, and a less prominent age cluster of 300–500 Ma. The remaining grains are of 500–700 Ma, 700–900 Ma, and 900–1050 Ma. Sample 16AD03D does not have grains younger than 205 Ma. Sample 16QS01D has two young age clusters (n = 2 and 4, respectively). The maximum depositional age of the Sewa Formation was determined to be 170.5 (+14.3/–14.1) Ma (n = 4, TuffZirc age) by the second youngest cluster (Dickinson and Gehrels, 2009). The two youngest zircon grains in sample 16QS01D are much younger than the Middle Jurassic depositional age of the Sewa Formation, possibly a result of Pb loss.

The nearly identical age spectra of samples 16QS01D and 16AD03D (Fig. 7) suggest that they have similar sediment sources. Grains of 205–305 Ma may be derived from the Hoh Xil terrane (Fig. 6I), the Kunlun terrane (Fig. 6J), or both. Because the two samples have very few Jurassic grains, we infer that the Sewa and Bang'ai formations received detritus mainly from the Hoh Xil and Kunlun terranes to the north, with negligible contribution from the magmatic arc (Fig. 6C), which was developed in the southern Qiangtang terrane contemporaneously.

Zircon grains from the two igneous clasts (16AD01I and 16AD07I; Figs. 2C and 3) in the Amdo Formation conglomerate beds show distinct oscillatory zoning with Th/U ratios ranging between 0.5 and 2, indicating their magmatic origins (Corfu et al., 2003). Their weighted mean ages are 180.7 ± 2.6 Ma (n = 28; Fig. 9A) and 176.9 ± 1.7 Ma (n = 29; Fig. 9C), respectively. These ages match only the ages of the Early Jurassic igneous rocks in the Amdo basement (Figs. 2A and 6B), suggesting that the conglomerate clasts in the Amdo Formation were sourced from the Amdo basement to the south. This predication is supported by studies of clast compositions and sandstone petrography (Fig. S2 [footnote 1]) (Sun, 2005).

Conglomerate clasts in the Amdo Formation include 70%–75% igneous rocks (rhyolite, dacite, andesite, trachyandesite, granite, granite porphyry, and tuff) and 25%–30% sedimentary rocks (chert, limestone, and mudstone) (Sun, 2005). The composition suggests that the clasts are most likely from the Early Jurassic magmatic arc developed in the Amdo basement (Guynn et al., 2006) and the deep-marine sedimentary rocks within the Amdo suture zone. The lack of sandstone clasts suggests that the Qiangtang terrane was probably not a major source for the Amdo Formation. Petrographic study of the Amdo Formation sandstones (Sun, 2005) also indicates a magmatic arc provenance, most likely the Early Jurassic arc in the Amdo basement. Although metamorphic rocks are also present in the Amdo basement, no metamorphic clasts were observed in the Amdo Formation. This is probably because metamorphism occurred only at middle crustal levels during the Early Jurassic in rocks that did not exhume until the Early Cretaceous (Guynn et al., 2006), and thus did not contribute to the Early Jurassic Amdo Formation.

CHRONOSTRATIGRAPHY

Unlike in the Yanshiping area, the Jurassic chronostratigraphy is not well constrained in the Amdo area. Previous studies concluded that both the Amdo

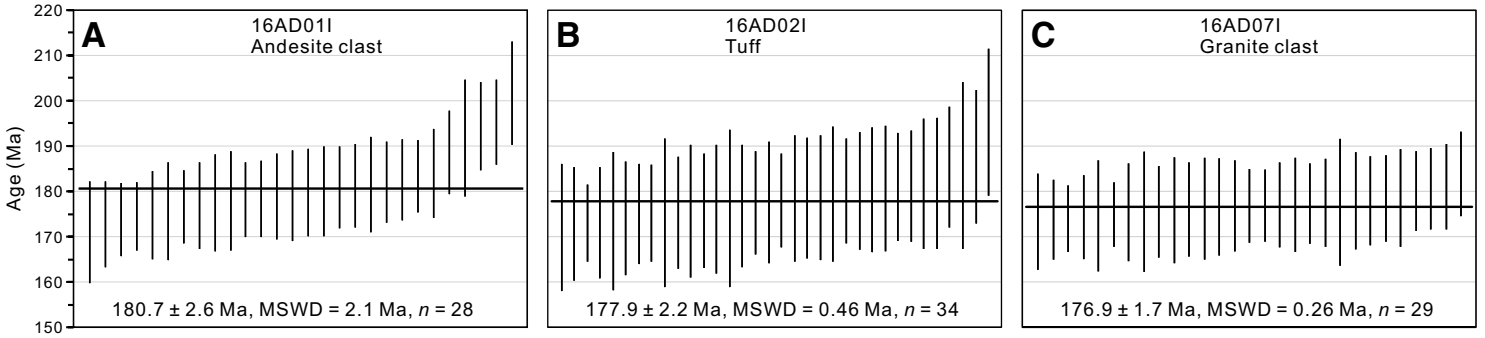

Figure 9. Weighted mean ages for two igneous clasts (A, sample 16AD01I; C, sample 16AD07I) and one tuff (B, sample 16AD02I) samples from the Amdo Formation. MSWD—mean square weighted deviation; *n*—numbers of zircon grains analyzed.

and Bang'ai formations are Late Jurassic to Early Cretaceous in age (Sun, 2005). Our new zircon U-Pb geochronology data suggest that the Amdo and Bang'ai formations were deposited during the Early and Middle Jurassic, respectively.

A tuff sample (16AD02I; Figs. 5C and 8B) was collected from the Amdo Formation (Figs. 2C and 3). Zircons from this sample have faint zoning and high Th/U ratios (0.4–1.6), indicating a magmatic origin (Corfu et al., 2003). The weighted mean age is 177.9 ± 2.2 Ma (n = 34; Fig. 9B), similar to the mean ages of the two volcanic clasts in the formation (Fig. 9A and 9C). A gabbro that is stratigraphically below the Amdo Formation and associated with the ophiolite near Amdo yields a zircon U-Pb age of 184 ± 2 Ma (Wang et al., 2016), providing a maximum depositional age for the Amdo Formation. Therefore, the Amdo Formation was deposited during the late Early Jurassic. Although the contact between the Amdo and Sewa formations cannot be observed in the field (Fig. 2A), we infer that the Amdo Formation was deposited earlier than the Sewa Formation because the middle–upper Amdo Formation was deposited in a subaerial braided river–alluvial fan environment (Sun, 2005), whereas the Sewa Formation and other Middle Jurassic strata in the Amdo-Yanshiping area were deposited in a shallow marine environment (Fig. 4). Long-term sea-level rise has been documented since the Bajocian (Fig. 3; Haq et al., 1987; Hallam, 1988), when Sewa Formation deposition began. Therefore, we infer that the Amdo Formation was deposited during the late Early to early Middle Jurassic, e.g., 184 Ma to >171 Ma.

We further conclude that the Bang'ai Formation was not Late Jurassic, but Middle Jurassic in age. If the formation was deposited during the Late Jurassic, we would expect abundant Jurassic zircons derived from the southern Qiangtang magmatic arc in the sandstone, similar to the observation made in the two samples from the Late Jurassic Xiali and Xueshan formations in the Yanshiping area (e.g., 150–200 Ma; Figs. 6G–6H). This expectation is based on the fact that the Amdo area is much closer to the magmatic arc than the Yanshiping area is. The lack of Jurassic zircons thus suggests that the Bang'ai Formation was deposited before the Late Jurassic. In addition, the detrital zircon age spectra (Figs. 6 and 7) and lithology (Fig. 4B) of the Bang'ai and Sewa formations are very similar, suggesting that the two formations were likely deposited during the same time (Fig. 3).

Based on the new geochronology data, we suggest that Jurassic deposition in the Amdo area initiated with the late Early Jurassic Amdo Formation, followed by the Middle Jurassic marine strata of the Sewa and Bang'ai formations, and ended with the late Middle Jurassic Buqu Formation (Fig. 3). Unlike the Yanshiping area, the Amdo area does not have Late Jurassic strata that are equivalent to the Xiali, Suowa, and Xueshan formations.

DISCUSSION

Late Early–Early Middle Jurassic Collision of the Amdo Basement with the Qiangtang Terrane

Previous studies have suggested that the Amdo basement experienced high-grade metamorphism during the Early Jurassic (Guynn et al., 2006; Zhang et al., 2012b; Zhang et al., 2014c). However, two different opinions exist concerning the origin of the metamorphism. Based on the observation that the amphibolite-facies metamorphism was coeval with the extensive emplacement of 185–170 Ma granitoids in the Amdo basement, Guynn et al. (2006) attributed both the metamorphism and magmatism to the development of a continental magmatic arc by the northward subduction of the Meso-Tethys oceanic lithosphere underneath the Amdo basement. Other studies reported ca. 190 Ma high-pressure granulite-facies metamorphism, which was interpreted to be a result of deep continental subduction of the Amdo basement beneath the Qiangtang terrane to ~50 km depth at ca. 190 Ma (Zhang et al., 2012b; Zhang et al., 2014c). These latter studies also interpreted the ca. 180 Ma amphibolite facies to be a result of retrograde metamorphism that occurred during return of the Amdo basement to mid-crustal levels (e.g., ~20 km), due to the breakoff

of a deeply subducted oceanic lithosphere slab that was previously attached to the Amdo basement (Zhang et al., 2014c).

The latter model of Zhang et al. (2012b) and Zhang et al. (2014c) infers that the Amdo basement collided with the Qiangtang terrane before 190 Ma and was at ~20 km depth at ca. 180 Ma. These inferences contradict our and previous (Sun, 2005) sedimentological and provenance results. The Amdo basement should have been at the Earth surface during the late Early–early Middle Jurassic to provide detritus for deposition of the Amdo Formation (i.e., 184–171 Ma; Fig. 10A). Our results agree with the model of Guynn et al. (2006) that suggests that both northward subduction of the Amdo basement beneath the Qiangtang terrane and subduction of the Meso-Tethys oceanic lithosphere beneath the Amdo basement were ongoing during the late Early–early Middle Jurassic (Fig. 10A).

Initial Lhasa-Qiangtang Collision at ca. 163 Ma

Our new provenance data suggest that the southern Qiangtang magmatic arc, produced by the northward subduction of the Meso-Tethys oceanic lithosphere, was submerged below sea level during the Middle Jurassic and provided very few Jurassic zircons to contemporaneous deposits (Fig. 10B). The arc was raised above sea level beginning in the earliest Late Jurassic (ca. 163 Ma), providing abundant Jurassic detritus to the Late Jurassic strata in the Yanshiping area (Fig. 10C). There are three potential causes for the uplift of the southern Qiangtang magmatic arc: (1) flat-slab subduction of the Meso-Tethys oceanic lithosphere; (2) significant growth of the magmatic arc due to increased magmatism; and/or (3) initial collision between the Lhasa and Qiangtang terranes. We preclude flat-slab subduction as a possible cause because this process would have led to a northward migration of arc magmatism, which has not been documented (Li et al., 2014; Liu et al., 2017; Hao et al., 2016, and references therein).

We prefer initial collision between the Lhasa and Qiangtang terranes (Fig. 10C, scenario 1) rather than increased arc magmatism (Fig. 10C, scenario 2) as the most plausible cause for uplift of the magmatic arc, for the following reasons. First, unlike the extensively exposed Gangdese magmatic arc in the southern Lhasa terrane (Ji et al., 2009), Middle and Late Jurassic magmatic rocks in the southern Qiangtang terrane are very limited, both spatially and volumetrically (Dewey et al., 1988; Liu et al., 2017). The small volume of Middle and Late Jurassic intrusions of the southern Qiangtang terrane does not suggest major growth in the magmatic arc. Second, paleomagnetic studies of the Middle and Late Jurassic strata in the Yanshiping area have shown that the paleolatitude of the southern Qiangtang terrane is indistinguishable from that of the northern Lhasa terrane during the Late Jurassic (Yan et al., 2016, and references therein). The Yanshiping area also experienced a change from clockwise rotation to counterclockwise rotation at ca. 162 Ma (Yan et al., 2016). The timing of this rotation is consistent with the first appearance of arc-derived detrital grains in the Xiali Formation (ca. 163 Ma). Furthermore, the prediction of ca. 163 Ma initial collision also agrees with the observation of Middle–Late Jurassic obduction of ophiolite fragments onto the northern margin of the Lhasa terrane near Amdo (Yin and Harrison, 2000). Taken together, these nearly synchronous changes at ca. 163 Ma in paleolatitude, sense of rotation, ophiolite obduction, as well as sediment provenance in the central Qiangtang terrane can be best interpreted as the result of the initial collision between the Lhasa and Qiangtang terranes.

The inference of the initial Lhasa-Qiangtang collision at ca. 163 Ma near Amdo is in line with a previous suggestion of a Middle–Late Jurassic east-west diachronous collision model (Yin and Harrison, 2000), although oceanic lithosphere might have existed between the two terranes until the Early Cretaceous, e.g., 131–121 Ma, near Gaize in the western Bangong suture zone (Baxter et al., 2009).

Our result argues against the early Late Cretaceous collision model. The evidence used for the Late Cretaceous collision model might be interpreted by alternative processes. On one hand, the 120–108 Ma basaltic rocks, which were previously thought to denote the presence of oceanic crust (Zhu et al., 2006; Liu et al., 2014; Zhang et al., 2014a; Fan et al., 2015), might have been derived from asthenospheric materials experiencing decompressional melting after the Lhasa-Qiangtang collision (Zhu et al., 2016). On the other hand, the 130–100 Ma intrusions found at the southern margin of Qiangtang might not have been produced during northward subduction of the Meso-Tethys ocean, but formed during collision of the Lhasa and Qiangtang terranes (Liu et al., 2017; Zhu et al., 2016). A useful analog for this is the India-Asia collision, the initiation of which is well documented to have been at ca. 59 Ma (Hu et al., 2016, and references therein), but magmatism persisted in various forms until the Miocene (Mo et al., 2007; Ji et al., 2009). An alternative explanation for the 130–100 Ma intrusions is that these rocks were produced by the flat-slab subduction of the Neo-Tethys oceanic lithosphere, which reached far north to the Bangong suture zone (Coulon et al., 1986).

Jurassic Successive Terrane Collisions in Central Tibet

We divide the Jurassic sedimentary-tectonic evolution of the south-central Qiangtang terrane and Bangong suture zone into three stages (Fig. 10).

During the late Early to early Middle Jurassic (184–171 Ma; Fig. 10A), the Amdo terrane collided with and subducted beneath the Qiangtang terrane, forming the Amdo suture. The majority of the Qiangtang terrane experienced erosion, and deposition was limited to the Amdo suture zone, where the fan delta– and alluvial fan–dominated Amdo Formation was deposited. At the same time, the Meso-Tethys oceanic lithosphere subducted northward beneath the Amdo basement, resulting in magmatism and metamorphism in only the Amdo basement, but not in the Qiangtang terrane (Guynn et al., 2006). This Early Jurassic arc magmatism provided igneous detritus and volcanic ash to the Amdo Formation.

During the Middle Jurassic (171–163 Ma; Fig. 10B), the integrated Qiangtang terrane and Amdo basement formed the continental shelf on the southern edge

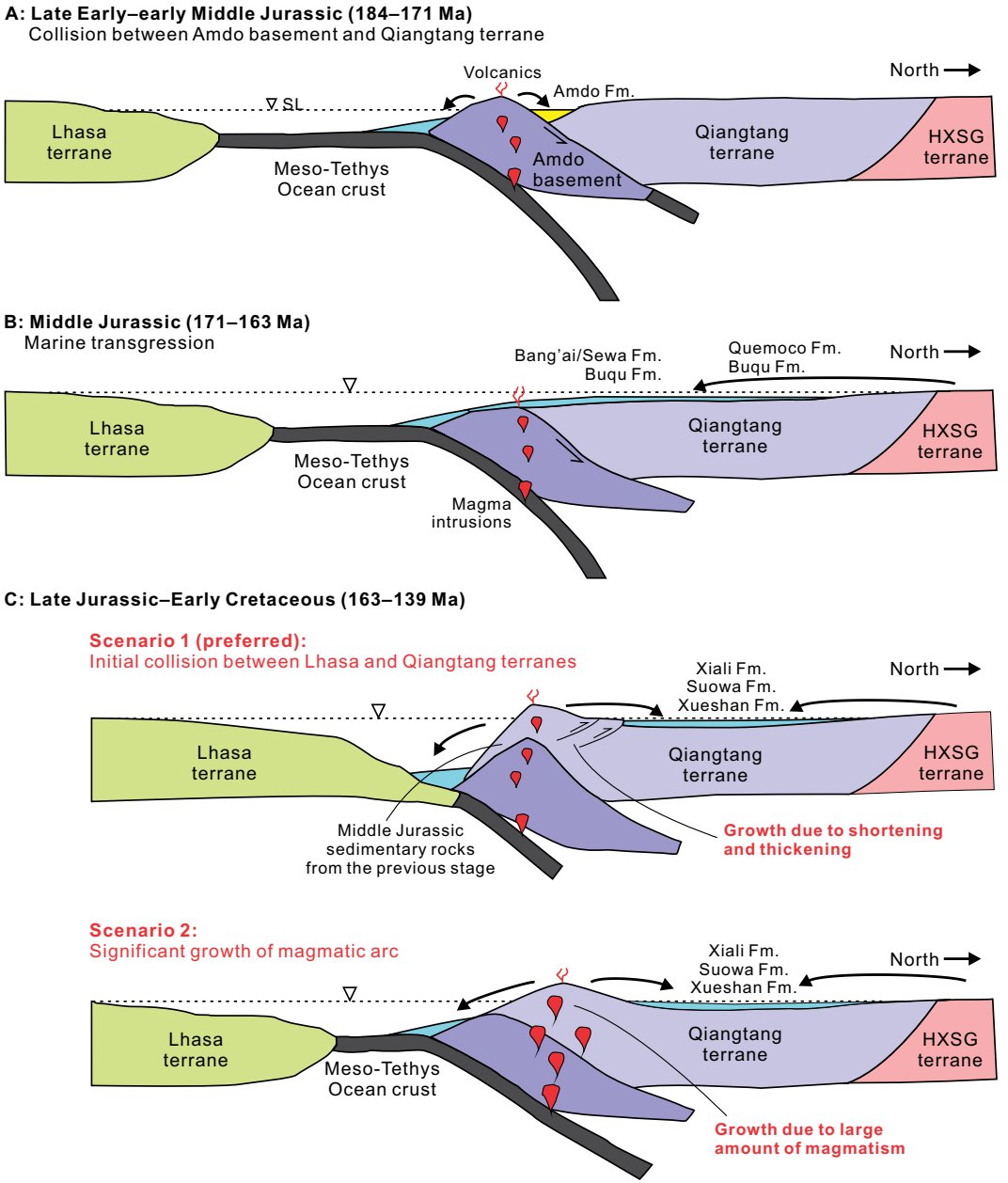

Figure 10. Schematic cross-sections showing the tectonic-sedimentary evolution of south-central Tibet during the late Early–early Middle Jurassic (A), Middle Jurassic (B), and Late Jurassic–Early Cretaceous (C). Between the two possible scenarios for the Late Jurassic–Early Cretaceous, scenario 1 is preferred (see text for detailed discussion). Thick black arrows show detritus transport routes. Note that during the Middle and Late Jurassic, the Amdo basement continued to subduct beneath the southern Qiangtang terrane. SL—sea level; yellow and blue colors represent subaerial and marine deposition, respectively. Fm.—Formation; HXSG—Hoh Xil–Songpan–Ganzi.

of the Asian continent because of sea-level rise (Fig. 3; Haq et al., 1987; Hallam, 1988). The Qiangtang basin was dominated by shallow and marginal marine deposition that received detritus mainly from the Hoh Xil and Kunlun terranes to the north. Continued northward subduction of the Meso-Tethys oceanic lithosphere produced a magmatic arc in the southern Qiangtang terrane. However, only a few Early–Middle Jurassic (200–160 Ma) zircons were observed in the Middle Jurassic sandstones (Figs. 6D and 6F), indicating that the magmatic arc was less active and probably submerged below sea level. The Amdo basement was also most likely covered by the Middle Jurassic shallow marine deposition.

After the early Late Jurassic, i.e., ca. 163 Ma, sea water retreated from the southern Qiangtang terrane, leading to a depositional hiatus in the Amdo area but a remnant marine basin in the central Qiangtang terrane. Because sea level continued to rise during the Middle–Late Jurassic (Hallam, 1988), recycling of zircon grains from the magmatic arc most likely represents surface uplift of the arc. Therefore, we suggest that during this stage, the southern Qiangtang magmatic arc was raised above sea level and contributed detritus to the Late Jurassic strata in the central Qiangtang terrane, along with the Hoh Xil and Kunlun terranes to the north (Fig. 10C). Although uplift of the magmatic arc may also be explained by a significant increase in arc magmatism (Fig. 10C, scenario 2), it is more likely caused by the initial collision between the Lhasa and Qiangtang terranes (Fig. 10C, scenario 1; see discussion in previous section). Full collision between the Lhasa and Qiangtang terranes probably occurred in the Early Cretaceous, evidenced by the cessation of marine sedimentation in the entire Qiangtang terrane (Fig. 3; Wang et al., 2001) and extensive Early Cretaceous deformation and shortening in the southern Qiangtang terrane (Kapp et al., 2005; Raterman et al., 2014).

CONCLUSIONS

We study the Jurassic sediment provenance and chronostratigraphy in the Amdo-Yanshiping area of the south-central Qiangtang terrane in order to reconstruct the Jurassic sedimentary-tectonic evolution of the central Tibetan Plateau. New detrital zircon and tuff ages suggest that the earliest Jurassic deposition in the area occurred in the late Early–early Middle Jurassic Amdo Formation, followed by Middle Jurassic marine siliciclastic and carbonate successions throughout the region. Although marine sedimentation extended into the Late Jurassic in the Yanshiping area in central Qiangtang, no Late Jurassic strata exist in the Amdo area in southern Qiangtang.

Late Early–early Middle Jurassic deposition in the study area occurred only in the Amdo suture zone, represented by the fan delta and alluvial fan deposition in the Amdo Formation that received detritus mainly from the Amdo basement to the south. Sediment provenance suggests that the Amdo basement collided with the Qiangtang terrane during the late Early–early Middle Jurassic. During the Middle Jurassic, continued sea-level rise transformed the Qiangtang terrane to a shallow marine environment, with deposition of both siliciclastic and carbonate rocks. The contemporaneous magmatic arc in southern Qiangtang was probably submerged below sea level and provided minimal detritus to deposits in the Amdo-Yanshiping area. The area received detritus mainly from the Hoh Xil and Kunlun terranes to the north. Starting in the early Late Jurassic, the southern Qiangtang magmatic arc was raised above sea level, causing a depositional hiatus in the Amdo area and providing detritus to the Late Jurassic marginal marine to deltaic deposits in the Yanshiping area.

We view the initial Lhasa-Qiangtang collision as the most plausible cause for the uplift of the southern Qiangtang magmatic arc at ca. 163 Ma, which is supported by the results of several previous studies (Yin and Harrison, 2000; Yan et al., 2016). In order to test the early Late Jurassic collision model, additional studies, such as structural analysis, are required to clarify whether there was extensive Late Jurassic thrusting in the Amdo region.

ACKNOWLEDGMENTS

We would like to thank Alex Pullen, Mark Pecha, Nicky Giesler, Dan Alberts, and Kojo Plange from the Arizona LaserChron Center for help with detrital zircon analysis. We thank the associate editor Mike Taylor and two reviewers, Jay Chapman and Ryan Leary, for constructive comments and suggestions. This research was supported by U.S. National Science Foundation grants (EAR-1211527 and EAR-1348005 to Garzione) and a National Science Foundation of China grant (40921120406 to Zhisheng An).

REFERENCES CITED

Bai, S., 1989, New recognition of the marine Jurassic strata in southwestern Qinghai: Dizhi Lunping, v. 35, p. 529–536 (in Chinese with English abstract).

Bai, Z.D., Xu, D.B., and Zhang, X.J., 2005, Geology of the Anduo County quadrangle: People's Republic of China Geological Map I46C004002, 1 sheet, scale 1:25,000 (in Chinese).

Baxter, A.T., Aitchison, J.C., and Zyabrev, S.V., 2009, Radiolarian age constraints on Mesotethyan ocean evolution, and their implications for development of the Bangong–Nujiang suture, Tibet: Journal of the Geological Society, v. 166, p. 689–694, https://doi.org/10.1144/0016-76492008-128.

BGMRQH (Bureau of Geology and Mineral Resources of Qinghai Province), 1997, Stratigraphy (Lithostratic) of Qinghai Province: Wuhan, China University of Geosciences Press, p. 275–285 (in Chinese).

Cai, F., Ding, L., Laskowski, A.K., Kapp, P., Wang, H., Xu, Q., and Zhang, L., 2016, Late Triassic paleogeographic reconstruction along the Neo-Tethyan Ocean margins, southern Tibet: Earth and Planetary Science Letters, v. 435, p. 105–114, https://doi.org/10.1016/j.epsl.2015.12.027.

Cheng, F., Fu, S., Jolivet, M., Zhang, C., and Guo, Z., 2016, Source to sink relation between the Eastern Kunlun Range and the Qaidam Basin, northern Tibetan Plateau, during the Cenozoic: Geological Society of America Bulletin, v. 128, p. 258–283, https://doi.org/10.1130/B31260.1.

Corfu, F., Hanchar, J.M., Hoskin, P.W., and Kinny, P., 2003, Atlas of zircon textures: Reviews in Mineralogy and Geochemistry, v. 53, p. 469–500, https://doi.org/10.2113/0530469.

Coulon, C., Maluski, H., Bollinger, C., and Wang, S., 1986, Mesozoic and Cenozoic volcanic rocks from central and southern Tibet: ^{39}Ar-^{40}Ar dating, petrological characteristics and geodynamical significance: Earth and Planetary Science Letters, v. 79, p. 281–302, https://doi.org/10.1016/0012-821X(86)90186-X.

Coward, M.P., Kidd, W.S.F., Yun, P., Shackleton, R.M., and Hu, Z., 1988, The structure of the 1985 Tibet geotraverse, Lhasa to Golmud: Philosophical Transactions of the Royal Society of London A: Mathematical, Physical and Engineering Sciences, v. 327, p. 307–333, https://doi.org/10.1098/rsta.1988.0131.

Dewey, J.F., Shackleton, R.M., Chang, C., and Sun, Y., 1988, The tectonic evolution of the Tibetan Plateau: Philosophical Transactions of the Royal Society of London A: Mathematical, Physical, and Engineering Sciences, v. 327, p. 379–413, https://doi.org/10.1098/rsta.1988.0135.

Dickinson, W.R., and Gehrels, G.E., 2009, Use of U-Pb ages of detrital zircons to infer maximum depositional ages of strata: A test against a Colorado Plateau Mesozoic database: Earth and Planetary Science Letters, v. 288, p. 115–125, https://doi.org/10.1016/j.epsl.2009.09.013.

Ding, L., Yang, D., Cai, F.L., Pullen, A., Kapp, P., Gehrels, G.E., Zhang, L.Y., Zhang, H.Q., Lai, Q.Z., Yue, Y.H., and Shi, R.D., 2013, Provenance analysis of the Mesozoic Hoh-Xil-Songpan-Ganzi turbidites in northern Tibet: Implications for the tectonic evolution of the eastern Paleo-Tethys Ocean: Tectonics, v. 32, p. 34–48, https://doi.org/10.1002/tect.20013.

England, P., and Searle, M., 1986, The Cretaceous-Tertiary deformation of the Lhasa block and its implications for crustal thickening in Tibet: Tectonics, v. 5, p. 1–14, https://doi.org/10.1029/TC005i001p00001.

Fan, J.J., Li, C., Xie, C.M., Wang, M., and Chen, J.W., 2015, Petrology and U-Pb zircon geochronology of bimodal volcanic rocks from the Maierze Group, northern Tibet: Constraints on the timing of closure of the Banggong–Nujiang Ocean: Lithos, v. 227, p. 148–160, https://doi.org/10.1016/j.lithos.2015.03.021.

Fang, X., Song, C., Yan, M., Zan, J., Liu, C., Sha, J., Zhang, W., Zeng, Y., Wu, S., and Zhang, D., 2016, Mesozoic litho- and magneto-stratigraphic evidence from the central Tibetan Plateau for megamonsoon evolution and potential evaporites: Gondwana Research, v. 37, p. 110–129, https://doi.org/10.1016/j.gr.2016.05.012.

Gehrels, G., Valencia, V., and Pullen, A., 2006, Detrital zircon geochronology by laser-ablation multicollector ICPMS at the Arizona LaserChron Center: Paleontological Society Papers, v. 12, p. 67–76.

Gehrels, G., Kapp, P., DeCelles, P., Pullen, A., Blakey, R., Weislogel, A., Ding, L., Guynn, J., Martin, A., McQuarrie, N., and Yin, A., 2011, Detrital zircon geochronology of pre-Tertiary strata in the Tibetan-Himalayan orogen: Tectonics, v. 30, TC5016, https://doi.org/10.1029/2011TC002868.

Guo, Z.J., Li, Y.T., Nan, Z.B., and Ye, H.F., 2008, Relationship between deformation structure and petroleum accumulation and preservation, Qiangtang Basin, Tibet: Petroleum Exploration and Development, v. 35, p. 563–568, https://doi.org/10.1016/S1876-3804(09)60089-6.

Guynn, J.H., Kapp, P., Pullen, A., Heizler, M., Gehrels, G., and Ding, L., 2006, Tibetan basement rocks near Amdo reveal "missing" Mesozoic tectonism along the Bangong suture, central Tibet: Geology, v. 34, p. 505–508, https://doi.org/10.1130/G22453.1.

Guynn, J., Kapp, P., Gehrels, G.E., and Ding, L., 2012, U-Pb geochronology of basement rocks in central Tibet and paleogeographic implications: Journal of Asian Earth Sciences, v. 43, p. 23–50, https://doi.org/10.1016/j.jseaes.2011.09.003.

Hallam, A., 1988, A reevaluation of Jurassic eustasy in the light of new data and the revised Exxon curve, *in* Wilgus, C.K., Hastings, B.S., Kendall, C.G.St.C., Posamentier, H.W., Ross, C.A., and van Wagoner, J.C., eds., Sea-Level Changes: An Integrated Approach: Society of Economic Paleontologists and Mineralogists Special Publication 42, p. 261–273, https://doi.org/10.2110/pec.88.01.0261.

Hao, L.L., Wang, Q., Wyman, D.A., Ou, Q., Dan, W., Jiang, Z.Q., Wu, F.Y., Yang, J.H., Long, X.P., and Li, J., 2016, Underplating of basaltic magmas and crustal growth in a continental arc: Evidence from Late Mesozoic intermediate–felsic intrusive rocks in southern Qiangtang, central Tibet: Lithos, v. 245, p. 223–242, https://doi.org/10.1016/j.lithos.2015.09.015.

Haq, B.U., Hardenbol, J., and Vail, P.R., 1987, Chronology of fluctuating sea levels since the Triassic: Science, v. 235, p. 1156–1167, https://doi.org/10.1126/science.235.4793.1156.

Hu, X., Garzanti, E., Wang, J., Huang, W., An, W., and Webb, A., 2016, The timing of India-Asia collision onset—Facts, theories, controversies: Earth-Science Reviews, v. 160, p. 264–299, https://doi.org/10.1016/j.earscirev.2016.07.014.

Huang, T.T., Xu, J.F., Chen, J.L., Wu, J.B., and Zeng, Y.C., 2016, Sedimentary record of Jurassic northward subduction of the Bangong-Nujiang Ocean: Insights from detrital zircons: International Geology Review, v. 59, p. 166–184, https://doi.org/10.1080/00206814.2016.1218801.

Ji, W.Q., Wu, F.Y., Chung, S.L., Li, J.X., and Liu, C.Z., 2009, Zircon U-Pb geochronology and Hf isotopic constraints on petrogenesis of the Gangdese batholith, southern Tibet: Chemical Geology, v. 262, p. 229–245, https://doi.org/10.1016/j.chemgeo.2009.01.020.

Kapp, P., Yin, A., Manning, C.E., Murphy, M., Harrison, T.M., Spurlin, M., Ding, L., Deng, X.G., and Wu, C.M., 2000, Blueschist-bearing metamorphic core complexes in the Qiangtang block reveal deep crustal structure of northern Tibet: Geology, v. 28, p. 19–22, https://doi.org/10.1130/0091-7613(2000)28<19:BMCCIT>2.0.CO;2.

Kapp, P., Yin, A., Manning, C.E., Harrison, T.M., Taylor, M.H., and Ding, L., 2003, Tectonic evolution of the early Mesozoic blueschist-bearing Qiangtang metamorphic belt, central Tibet: Tectonics, v. 22, 1043, https://doi.org/10.1029/2002TC001383.

Kapp, P., Yin, A., Harrison, T.M., and Ding, L., 2005, Cretaceous-Tertiary shortening, basin development, and volcanism in central Tibet: Geological Society of America Bulletin, v. 117, p. 865–878, https://doi.org/10.1130/B25595.1.

Kapp, P., DeCelles, P.G., Gehrels, G.E., Heizler, M., and Ding, L., 2007a, Geological records of the Lhasa-Qiangtang and Indo-Asian collisions in the Nima area of central Tibet: Geological Society of America Bulletin, v. 119, p. 917–933, https://doi.org/10.1130/B26033.1.

Kapp, P., DeCelles, P.G., Leier, A.L., Fabijanic, J.M., He, S., Pullen, A., Gehrels, G.E., and Ding, L., 2007b, The Gangdese retroarc thrust belt revealed: GSA Today, v. 17, no. 7, p. 4–9, https://doi.org/10.1130/GSAT01707A.1.

Leeder, M.R., Smith, A.B., and Yin, J.X., 1988, Sedimentology, palaeoecology and palaeoenvironmental evolution of the 1985 Lhasa to Golmud Geotraverse: Philosophical Transactions of the Royal Society of London A: Mathematical, Physical, and Engineering Sciences, v. 327, p. 107–143, https://doi.org/10.1098/rsta.1988.0123.

Leier, A.L., Kapp, P., Gehrels, G., and DeCelles, P.G., 2007, Detrital zircon geochronology of Carboniferous–Cretaceous strata in the Lhasa terrane, Southern Tibet: Basin Research, v. 19, p. 361–378, https://doi.org/10.1111/j.1365-2117.2007.00330.x.

Li, C., Cheng, L.R., and Hu, K., 1995, Study on the paleo-Tethys suture zone of Lungmu Co-Shuanghu, Tibet: Beijing, Geological Publication House, 131 p. (in Chinese).

Li, G.M., Li, J.X., Zhao, J.X., Qin, K.Z., Cao, M.J., and Evans, N.J., 2015, Petrogenesis and tectonic setting of Triassic granitoids in the Qiangtang terrane, central Tibet: Evidence from U-Pb ages, petrochemistry and Sr-Nd-Hf isotopes: Journal of Asian Earth Sciences, v. 105, p. 443–455, https://doi.org/10.1016/j.jseaes.2015.02.017.

Li, J., and Batten, D.J., 2004, Early Cretaceous palynofloras from the Tanggula Mountains of the northern Qinghai-Xizang (Tibet) Plateau, China: Cretaceous Research, v. 25, p. 531–542, https://doi.org/10.1016/j.cretres.2004.04.005.

Li, J., Riding, J.B., Cheng, J., and He, C., 2011, Latest Jurassic–earliest Cretaceous (Tithonian–Berriasian) dinoflagellate cysts from the Yanshiping Group of the northern Qinghai-Xizang Plateau (Tibet), western China: Review of Palaeobotany and Palynology, v. 166, p. 38–45, https://doi.org/10.1016/j.revpalbo.2011.04.007.

Li, J.X., Qin, K.Z., Li, G.M., Richards, J.P., Zhao, J.X., and Cao, M.J., 2014, Geochronology, geochemistry, and zircon Hf isotopic compositions of Mesozoic intermediate–felsic intrusions in central Tibet: Petrogenetic and tectonic implications: Lithos, v. 198–199, p. 77–91, https://doi.org/10.1016/j.lithos.2014.03.025.

Li, S., Ding, L., Guilmette, C., Fu, J., Xu, Q., Yue, Y., and Henrique-Pinto, R., 2017, The subduction-accretion history of the Bangong-Nujiang Ocean: Constraints from provenance and geochronology of the Mesozoic strata near Gaize, central Tibet: Tectonophysics, v. 702, p. 42–60, https://doi.org/10.1016/j.tecto.2017.02.023.

Li, Y., Wang, C.S., Yi, H.S., Shi, H., Lin, J.H., Zhu, L.D., and Li, X.H., 2001, Fill models of the Qiangtang composite foreland basin in Qinghai-Xizang Plateau, China: Acta Sedimentologica Sinica, v. 19, p. 20–27 (in Chinese with English abstract).

Li, Y., Li, Y.L., and Duan, Z.M., 2005, Geology of the Wenquanbingzhan quadrangle: People's Republic of China Geological Map I46C003002, 1 sheet, scale 1:25,000 (in Chinese).

Liu, D., Shi, R., Ding, L., Huang, Q., Zhang, X., Yue, Y., and Zhang, L., 2017, Zircon U-Pb age and Hf isotopic compositions of Mesozoic granitoids in southern Qiangtang, Tibet: Implications for the subduction of the Bangong–Nujiang Tethyan Ocean: Gondwana Research, v. 41, p. 157–172, https://doi.org/10.1016/j.gr.2015.04.007.

Liu, D.L., Shi, R.D., Ding, L., and Zou, H.B., 2018, Late Cretaceous transition from subduction to collision along the Bangong-Nujiang Tethys: New volcanic constraints from central Tibet: Lithos, v. 296–299, p. 452–470, https://doi.org/10.1016/j.lithos.2017.11.012.

Liu, W.L., Xia, B., Zhong, Y., Cai, J.X., Li, J.F., Liu, H.F., Cai, Z.R., and Sun, Z.L., 2014, Age and composition of the Rebang Co and Julu ophiolites, central Tibet: Implications for the evolution of the Bangong Meso-Tethys: International Geology Review, v. 56, p. 430–447, https://doi.org/10.1080/00206814.2013.873356.

Ludwig, K., and Mundil, R., 2002, Extracting reliable U-Pb ages and errors from complex populations of zircons from Phanerozoic tuffs: Geochimica et Cosmochimica Acta, v. 66 (Supplement 1), p. 463.

Matte, P., Tapponnier, P., Arnaud, N., Bourjot, L., Avouac, J.P., Vidal, P., Liu, Q., Pan, Y.S., and Wang, Y., 1996, Tectonics of Western Tibet, between the Tarim and the Indus: Earth and Planetary Science Letters, v. 142, p. 311–330, https://doi.org/10.1016/0012-821X(96)00086-6.

Metcalfe, I., 1996, Gondwanaland dispersion, Asian accretion and evolution of eastern Tethys: Australian Journal of Earth Sciences, v. 43, p. 605–623, https://doi.org/10.1080/08120099608728282.

Mo, X., Hou, Z., Niu, Y., Dong, G., Qu, X., Zhao, Z., and Yang, Z., 2007, Mantle contributions to crustal thickening during continental collision: Evidence from Cenozoic igneous rocks in southern Tibet: Lithos, v. 96, p. 225–242, https://doi.org/10.1016/j.lithos.2006.10.005.

Murphy, M.A., Yin, A., Harrison, T.M., Dürr, S.B., Chen, Z., Ryerson, F.J., Kidd, W.S.F., Wang, X., and Zhou, X. 1997, Did the Indo-Asian collision alone create the Tibetan plateau?: Geology, v. 25, p. 719–722, https://doi.org/10.1130/0091-7613(1997)025<0719:DTIACA>2.3.CO;2.

Pullen, A., Kapp, P., Gehrels, G.E., Vervoort, J.D., and Ding, L., 2008, Triassic continental subduction in central Tibet and Mediterranean-style closure of the Paleo-Tethys Ocean: Geology, v. 36, p. 351–354, https://doi.org/10.1130/G24435A.1.

Pullen, A., Kapp, P., Gehrels, G.E., Ding, L., and Zhang, Q., 2011, Metamorphic rocks in central Tibet: Lateral variations and implications for crustal structure: Geological Society of America Bulletin, v. 123, p. 585–600, https://doi.org/10.1130/B30154.1.

Pullen, A., Ibáñez-Mejía, M., Gehrels, G.E., Ibáñez-Mejía, J.C., and Pecha, M., 2014, What happens when *n*=1000? Creating large-*n* geochronological datasets with LA-ICP-MS for geologic investigations: Journal of Analytical Atomic Spectrometry, v. 29, p. 971–980, https://doi.org/10.1039/C4JA00024B.

Raterman, N.S., Robinson, A.C., and Cowgill, E.S., 2014, Structure and detrital zircon geochronology of the Domar fold-thrust belt: Evidence of pre-Cenozoic crustal thickening of the western Tibetan Plateau, *in* Nie, J., Horton, B.K., and Hoke, G.D., eds., Toward an Improved Understanding of Uplift Mechanisms and the Elevation History of the Tibetan Plateau: Geological Society of America Special Paper 507, p. 89–104, https://doi.org/10.1130/2014.2507(05).

Song, C., Zeng, Y., Yan, M., Wu, S., Fang, X., Bao, J., Zan, J., and Liu, X., 2016, Magnetostratigraphy of the Middle-Upper Jurassic sedimentary sequences at Yanshiping, Qiangtang Basin, China: Geophysical Journal International, v. 206, p. 1847–1863, https://doi.org/10.1093/gji/ggw199.

Stacey, J.S., and Kramers, J.D., 1975, Approximation of terrestrial lead isotope evolution by a two-stage model: Earth and Planetary Science Letters, v. 26, p. 207–221, https://doi.org/10.1016/0012-821X(75)90088-6.

Sun, L.X., 2005, Late Jurassic–Cretaceous sedimentary response to collision process in middle Bangonghu–Nujiang suture [Ph.D. thesis]: Beijing, China University of Geosciences, 121 p.

Vermeesch, P., Resentini, A., and Garzanti, E., 2016, An R package for statistical provenance analysis: Sedimentary Geology, v. 336, p. 14–25, https://doi.org/10.1016/j.sedgeo.2016.01.009.

Wang, B.D., Wang, L.Q., Chung, S.L., Chen, J.L., Yin, F.G., Liu, H., Li, X.B., and Chen, L.K., 2016, Evolution of the Bangong–Nujiang Tethyan ocean: Insights from the geochronology and geochemistry of mafic rocks within ophiolites: Lithos, v. 245, p. 18–33, https://doi.org/10.1016/j.lithos.2015.07.016.

Wang, C.S., Yi, H.S., Li, Y., Deng, B., and Liu, D.Z., 2001, The geological evolution and prospective oil and gas assessment of the Qiangtang basin in northern Tibetan Plateau: Beijing, Geological Publishing House, 226 p.

Wang, J., Ding, J., and Wang, C., 2010a, Potential analysis and geological survey of the hydrocarbon resources in Tibetan Plateau: Beijing, Geological Publishing House, 254 p. (in Chinese).

Wang, J., Fu, X.G., Tan, F.W., Chen, M., and He, J.L., 2010b, A new sedimentary model for the Qiangtang Basin: Acta Sedimentologica Sinica, v. 28, p. 884–893.

Wang, L.Q., and Pan, G.T., 2012, Geologic map of Qinghai-Xizang (Tibet) Plateau and adjacent areas: Beijing, Geological Publishing House, one sheet, scale 1:1,500,000.

Yan, M., Zhang, D., Fang, X., Ren, H., Zhang, W., Zan, J., Song, C., and Zhang, T., 2016, Paleomagnetic data bearing on the Mesozoic deformation of the Qiangtang Block: Implications for the evolution of the Paleo- and Meso-Tethys: Gondwana Research, v. 39, p. 292–316, https://doi.org/10.1016/j.gr.2016.01.012.

Yang, Z.Y., and Yin, J.R., 1988, On Jurassic strata of southern Qinghai province: Geoscience, v. 2, p. 278–292 (in Chinese with English abstract).

Yao, H.Z., Zhang, R.J., Duan, Q.F., Sheng, X.C., Niu, Z.J., Wang, J.X., and Wu, J.H., 2011, Jurassic rocks, bivalves, and depositional environments of the source area of the Yangtze River, Qinghai Province, western China: Science China Earth Sciences, v. 54, https://doi.org/10.1007/s11430-011-4223-0 (in Chinese).

Yin, A., and Harrison, T.M., 2000, Geologic evolution of the Himalayan-Tibetan orogen: Annual Review of Earth and Planetary Sciences, v. 28, p. 211–280, https://doi.org/10.1146/annurev.earth.28.1.211.

Yin, J.R., 1987, New materials of Jurassic bivalves from the northern slope of Tanggula Mountains: Geoscience (Journal of the Graduate School of China University of Geosciences), v. 1, p. 327–337 (in Chinese with English abstract).

Yin, J.R., 2005, Middle Jurassic (Bathonian-Callovian) ammonites from the Amdo area, northern Tibet: Acta Palaeontologica Sinica, v. 44, p. 1–16 (in Chinese with English abstract).

Zhang, K.J., Cai, J.X., Zhang, Y.X., and Zhao, T.P., 2006a, Eclogites from central Qiangtang, northern Tibet (China) and tectonic implications: Earth and Planetary Science Letters, v. 245, p. 722–729, https://doi.org/10.1016/j.epsl.2006.02.025.

Zhang, K.J., Zhang, Y.X., Li, B., Zhu, Y.T., and Wei, R.Z., 2006b, The blueschist-bearing Qiangtang metamorphic belt (northern Tibet, China) as an in situ suture zone: Evidence from geochemical comparison with the Jinsa suture: Geology, v. 34, p. 493–496, https://doi.org/10.1130/G22404.1.

Zhang, K.J., Zhang, Y.X., Tang, X.C., and Xia, B., 2012a, Late Mesozoic tectonic evolution and growth of the Tibetan plateau prior to the Indo-Asian collision: Earth-Science Reviews, v. 114, p. 236–249, https://doi.org/10.1016/j.earscirev.2012.06.001.

Zhang, K.J., Xia, B., Zhang, Y.X., Liu, W.L., Zeng, L., Li, J.F., and Xu, L.F., 2014a, Central Tibetan Meso-Tethyan oceanic plateau: Lithos, v. 210–211, p. 278–288, https://doi.org/10.1016/j.lithos.2014.09.004.

Zhang, L.Y., Ding, L., Pullen, A., Xu, Q., Liu, D.L., Cai, F.L., Yue, Y.H., Lai, Q.Z., Shi, R.D., and Ducea, M.N., 2014b, Age and geochemistry of western Hoh-Xil-Songpan-Ganzi granitoids, northern Tibet: Implications for the Mesozoic closure of the Paleo-Tethys ocean: Lithos, v. 190–191, p. 328–348, https://doi.org/10.1016/j.lithos.2013.12.019.

Zhang, X., Shi, R., Huang, Q., Liu, D., Gong, X., Chen, S., Wu, K., Yi, G., Sun, Y., and Ding, L., 2014c, Early Jurassic high-pressure metamorphism of the Amdo terrane, Tibet: Constraints from zircon U-Pb geochronology of mafic granulites: Gondwana Research, v. 26, p. 975–985, https://doi.org/10.1016/j.gr.2013.08.003.

Zhang, Z.M., Dong, X., Liu, F., Lin, Y.H., Yan, R., and Santosh, M., 2012b, Tectonic evolution of the Amdo terrane, central Tibet: Petrochemistry and zircon U-Pb geochronology: The Journal of Geology, v. 120, p. 431–451, https://doi.org/10.1086/665799.

Zhu, D.C., Pan, G.T., Mo, X.X., Wang, L.Q., Zhao, Z.D., Liao, Z.L., Geng, Q.R., and Dong, G.C., 2006, Identification for the Mesozoic OIB-type basalts in Central Qinghai–Tibetan Plateau: Geochronology, geochemistry and their tectonic setting: Acta Geologica Sinica, v. 80, p. 1312–1328 (in Chinese with English abstract).

Zhu, D.C., Zhao, Z.D., Niu, Y.L., Dilek, Y., and Mo, X.X., 2011, Lhasa terrane in southern Tibet came from Australia: Geology, v. 39, p. 727–730, https://doi.org/10.1130/G31895.1.

Zhu, D.C., Zhao, Z.D., Niu, Y.L., Dilek, Y., Hou, Z.Q., and Mo, X.X., 2013, The origin and pre-Cenozoic evolution of the Tibetan Plateau: Gondwana Research, v. 23, p. 1429–1454, https://doi.org/10.1016/j.gr.2012.02.002.

Zhu, D.C., Li, S.M., Cawood, P.A., Wang, Q., Zhao, Z.D., Liu, S.A., and Wang, L.Q., 2016, Assembly of the Lhasa and Qiangtang terranes in central Tibet by divergent double subduction: Lithos, v. 245, p. 7–17, https://doi.org/10.1016/j.lithos.2015.06.023.